Disturbance in Hebbian-like spinogenesis blunted learning-induced modulation in the number and spatial distribution of dendritic spines

Maura Ferrer-Ferrer
German Centre for Neurodegenerative Diseases Site Magdeburg: Deutsches Zentrum fur Neurodegenerative Erkrankungen Standort Magdeburg

Shaobo Jia
German Centre for Neurodegenerative Diseases Site Magdeburg: Deutsches Zentrum fur Neurodegenerative Erkrankungen Standort Magdeburg

Rahul Kaushik
German Centre for Neurodegenerative Diseases Site Magdeburg: Deutsches Zentrum fur Neurodegenerative Erkrankungen Standort Magdeburg

Stepan Aleshin
German Centre for Neurodegenerative Diseases Site Magdeburg: Deutsches Zentrum fur Neurodegenerative Erkrankungen Standort Magdeburg

Jenny Schneeberg
German Centre for Neurodegenerative Diseases Site Magdeburg: Deutsches Zentrum fur Neurodegenerative Erkrankungen Standort Magdeburg

Andrey Mironov
German Centre for Neurodegenerative Diseases Site Magdeburg: Deutsches Zentrum fur Neurodegenerative Erkrankungen Standort Magdeburg

Motahareh Safari
German Centre for Neurodegenerative Diseases Site Magdeburg: Deutsches Zentrum fur Neurodegenerative Erkrankungen Standort Magdeburg

Renato Frischknecht
Friedrich-Alexander University Erlangen-Nuremberg: Friedrich-Alexander-Universitat Erlangen-Nurnberg

Oleg Senkov
German Centre for Neurodegenerative Diseases Site Magdeburg: Deutsches Zentrum fur Neurodegenerative Erkrankungen Standort Magdeburg

Alexander Dityatev (✉ alexander.dityatev@dzne.de)
German Centre for Neurodegenerative Diseases Site Magdeburg: Deutsches Zentrum fur Neurodegenerative Erkrankungen Standort Magdeburg https://orcid.org/0000-0002-0472-0553

Research Article

Keywords: Extracellular proteolysis, Neurotrypsin, Agrin, Dendritic spine, Synaptic plasticity, Learning and memory, Hebbian rule

Posted Date: June 24th, 2022

DOI: https://doi.org/10.21203/rs.3.rs-1740340/v1

Version of Record: A version of this preprint was published at Cellular and Molecular Life Sciences on March 5th, 2023. See the published version at https://doi.org/10.1007/s00018-023-04720-z.

Abstract

Neurotrypsin (NT) is a neuronal trypsin-like serine protease whose mutations cause severe mental retardation in humans. NT is activated by Hebbian-like conjunction of pre- and postsynaptic activities, which promotes the formation of dendritic filopodia via proteolytic cleavage of the proteoglycan agrin. Here, we investigated the functional importance of this mechanism for synaptic plasticity, learning and extinction of memory. We report that juvenile neurotrypsin-deficient ($NT^{-/-}$) mice exhibit impaired long-term potentiation induced by a spaced stimulation protocol designed to probe the generation of new filopodia and their conversion into functional synapses. Behaviorally, juvenile $NT^{-/-}$ mice show impaired contextual fear memory and have a sociability deficit. The latter persists in aged $NT^{-/-}$ mice, which, unlike juvenile mice, show normal recall but impaired extinction of contextual fear memories. Structurally, juvenile mutants exhibit significantly reduced spine density in the CA1 region, fewer thin spines and no modulation in the number and spatial distribution of dendritic spines following fear conditioning and extinction in contrast to wild-type littermates. Spine loss in $NT^{-/-}$ mice is abrogated by *in vivo* delivery of adeno-associated virus expressing an NT-generated fragment of agrin, agrin-22, but not by a shorter fragment, agrin-15. Moreover, agrin-22 co-aggregates with pre- and postsynaptic terminals immunopositive for vesicular glutamate transporter 1 and postsynaptic density protein PSD95 and dramatically increases the size of synaptic puncta, suggesting that agrin-22 supports the growth and/or clustering of excitatory synapses *in vivo*.

Introduction

Multiple studies have implicated the role of extracellular proteases in synaptic plasticity, learning and memory (Ferrer-Ferrer & Dityatev, 2018; Sonderegger & Matsumoto-Miyai, 2014). Neurotrypsin (NT), a neuronal trypsin-like serine protease, has been recognized to play an essential role in cognitive brain function due to a 4-nucleotide deletion in the PRSS12 gene of the human chromosome 4q, which results in an earlier stop codon and the production of a truncated protein leading to severe mental retardation in humans (Molinari et al., 2002). In the adult central nervous system (CNS) of humans, NT mRNA is highly expressed in the hippocampus (particularly in the subiculum and pyramidal cells of the CA1 region), cerebral cortex and amygdala (Gschwend et al., 1997). In the developing mouse brain, postnatal NT mRNA is strongly expressed in the cortex and hippocampus, reaching its peak expression during neural development and correlating with periods of synaptogenesis (Wolfer et al., 2001). By electron microscopy, NT was localized at the presynaptic terminals of human cortical synapses (Molinari et al., 2002). Live imaging studies in cultured hippocampal neurons revealed that NT is recruited and released presynaptically in an activity-dependent manner (Frischknecht et al., 2008). Interestingly, the proteolytic activity of NT requires coincident activation of NMDA receptors; i.e., its activation occurs in a Hebbian manner (Matsumoto-Miyai et al., 2009). At present, the only known proteolytic substrate of NT is the proteoglycan agrin. Synaptic agrin is cleaved by NT at two sites, yielding a 110 kDa N-terminal fragment, a 90 kDa internal fragment, and a 22 kDa C-terminal fragment (Stephan et al., 2008). In rodent brain slices, activity-dependent exocytosis of NT from presynaptic terminals—followed by agrin cleavage—

induces the formation of dendritic filopodia. This is in line with the finding that in NT knockout ($NT^{-/-}$) brain slices, no activity-dependent generation of dendritic filopodia is observed. However, activity-dependent formation of filopodia in slices could be rescued by application of agrin-22 but not agrin-90 fragments (Matsumoto-Miyai et al., 2009). The clinical relevance of this signaling mechanism is supported by a recent study showing that in a mouse model of infantile neuronal ceroid lipofuscinosis, in which the mice are deficient in ceroid lipofuscinosis neuronal-1 (Cln1), NT activity is suppressed due to upregulation of its inhibitor serpina1. A deficit in agrin-22 in this mutant may explain the synaptic dysfunctions characteristic of this disease (Peng et al., 2015).

Previous work has reported that the level of conventional theta-burst stimulation (TBS)-induced LTP is normal in hippocampal slices from $NT^{-/-}$ mice (Matsumoto-Miyai et al., 2009). However, the conventional protocol is not suited to detect enhancement of synaptic transmission due to the formation of new spines, as nascent spines are mostly silent due to a lack of AMPA receptors (Durand et al., 1996; Isaac et al., 1995; Liao et al., 1995; Petralia et al., 1999). It is plausible to assume, however, that the newly generated silent synapses, induced by agrin in response to the first TBS of presynaptic axons could become potentiated in the response to the second TBS applied 1 h after the first TBS. This time interval is necessary for the recruitment of postsynaptic density components to nascent synapses, which can be used as a scaffold for the recruitment of AMPA receptors (Kramár et al., 2012). Importantly, maturation of activity-induced filopodia-like dendritic protrusions into stable and functional spines with postsynaptic density can be observed *in vivo* and is essential for learning and memory formation (Harris, 2020).

Here, we investigated the functional importance of NT in this process *in vivo*. We found that $NT^{-/-}$ mice have an impairment of a specific form of long-term potentiation dependent on filopodia generation and their conversion into functional synapses. Behaviorally, $NT^{-/-}$ mice have shown deficits in contextual fear memory and sociability compared to their $NT^{+/+}$ littermates, suggesting an essential role of NT in regulating multiple aspects of higher cognitive functions in the brain. Morphological analysis revealed significantly reduced spine density in $NT^{-/-}$ mice. Furthermore, $NT^{-/-}$ mice have shown a lower proportion of thin/filopodia-like spines, in line with the hypothesis that NT may specifically affect filopodia formation.

Results

Contribution of neurotrypsin to synaptic plasticity in juvenile mice

First, we investigated the importance of NT-dependent spinogenesis for functional long-term synaptic plasticity underlying learning and memory. We used a “spaced” protocol for the induction of LTP and applied two 1-h spaced TBSs (Kramár et al., 2012). The first TBS was supposed to promote filopodia generation, while the second TBS may convert silent synapses into functional synapses by recruitment of AMPA receptors. As NT is expressed in the hippocampus, we tested spaced LTP in $NT^{+/+}$ and $NT^{-/-}$ juvenile mice at CA3-CA1 synapses (Figure 1).

We found that after induction of LTP by one TBS, the levels of potentiation were similar in both genotypes ($p_{genotype} = 0.383$, $F_{(1,19)} = 0.798$; $p_{genotype\ x\ time} = 1.000$, $F_{(717, 13623)} = 0.610$; Figure 1C, D). Application of the second TBS (TBS2) further increased the level of LTP in $NT^{+/+}$ but not in $NT^{-/-}$ mice ($p_{genotype} = 0.010$, $F_{(1,17)} = 8.280$; $p_{genotype\ x\ time} < 0.001$, $F_{(537,9129)} = 2.902$; Fig.1C, D). Overall, these results indicated that mice lacking NT showed no additional potentiation after TBS2, unlike control mice. These observations suggested that a new population of synapses induced by the NT-agrin signaling pathway by TBS1 could be potentiated by TBS2.

Role of neurotrypsin in contextual fear conditioning in juvenile mice

Previous experiments have implicated NT in hippocampal plasticity (Matsumoto-Miyai et al., 2009). To match the spaced LTP protocol at the behavioral level, we designed a protocol of spaced contextual fear conditioning (CFC) and extinction in which 6 foot shocks were applied in the conditioned context (CC+), divided into two learning sessions (3x + 3x) with a 1 h-interval delay between both sessions (Figure 2A). To evaluate fear memory, we measured the freezing response (total freezing time divided to trial duration) in the conditioned context (CC+) and in the neutral context (CC-) on day 2 (recall d2). To examine memory extinction, we analyzed freezing levels at day 9 (recall d9) after 9x extinction sessions in CC+ to erase conditioned fear. Monitoring the freezing response in the CC- allowed us to measure the mice's ability to differentiate between both contexts.

The results indicated that NT deficiency did not affect the level of spontaneous freezing before CFC at day 0 (training) in either the CC- or CC+ ($p_{genotype} = 0.405$, $F_{(1,21)} = 0.720$; $p_{genotype\ x\ context} = 0.417$, $F_{(1,20)} = 0.688$; Figure 2C). This freezing level shown by mice before CFC was typical for the exploration of novel environments in mice. Moreover, we assessed anxiety levels and general locomotor activity in the open field test. The results showed that NT deficiency altered neither general locomotor activity ($p = 0.540$; $NT^{-/-}$: 14.4 ± 1.1 m *vs.* $NT^{+/+}$: 15.3 ± 1.0 m; Figure S1D) nor anxiety levels ($p = 0.479$; $NT^{-/-}$: 34.2 ± 3.9 % *vs.* $NT^{+/+}$: 30.6 ± 3.0 %; Figure S1A). Additionally, the levels of freezing immediately after unconditioned stimuli were not different between genotypes ($p_{genotype} = 0.359$, $F_{(1,21)} = 0.880$, $p_{genotype\ x\ stimulus} = 0.250$, $F_{(5,105)} = 1.347$; Figure 2D).

Analysis of memory recall revealed that both groups of mice were able to distinguish between the CC+ and CC- contexts on d2 (two-way repeated measures ANOVA: $p_{context} < 0.0001$, $F_{(1,21)} = 92.929$; $p_{genotype} = 0.651$, $F_{(1,21)} = 0.210$; $p_{time\ x\ genotype} = 0.031$, $F_{(1,21)} = 5.323$; $p < 0.001$ for both $NT^{+/+}$ and $NT^{-/-}$ mice, respectively, Holm-Sidak *post hoc* test; Figure 2F left). During extinction sessions from day 5 to day 7, the freezing time in CC+ of both group gradually reduced ($p_{session} < 0.001$, $F_{(8,168)} = 7.13$), but there was not statistical difference detected between genotypes ($p_{genotype} = 0.469$, $F_{(1,21)} = 0.545$; $p_{genotype\ x\ session} = 0.245$, $F_{(8,168)} = 1.303$; Figure 2E). The fear response reduced to similar levels in all genotypes ($p_{genotype} = 0.416$, $F_{(1,21)} = 0.688$) and contexts ($p_{context} = 0.312$, $F_{(1,21)} = 1.074$) after the fear extinction protocol at recall on d9 (Figure 2F right). However, $NT^{-/-}$ mice appeared to be less efficient in discriminating between contexts during fear memory retrieval on day 2 ($p = 0.026$, Holm-Sidak *post hoc* test; Figure 2G). To

test whether impaired context discrimination was due to impaired visual function in $NT^{-/-}$ mice, we subjected these mice to the novel object recognition test (NORT) that critically depends on visual discrimination. As $NT^{-/-}$ mice stayed longer near novel rather than familiar objects in NORT (73.6 ± 13.6 s *vs.* 39.9± 12.5 s, $p = 0.0073$; Figure S1G), similar to $NT^{+/+}$ mice (65.7 ± 8.6 s *vs.* 38.8± 6.8 s, $p = 0.00007$; Figure S1G left), it appeared that they have normal visual function and form object recognition memory normally (discrimination ratio: $NT^{-/-}$: 42.1 ± 7.8 % *vs.* $NT^{+/+}$: 42.8 ± 4.6 %, $p = 0.937$; Figure S1H).

In these experiments, we used a strong CFC protocol, which resulted in only a mild difference between genotypes in the discrimination between contexts. To clarify whether this was due to a ceiling/saturation of CFC in both genotypes, we designed a milder CFC protocol with 3x foot shocks and single-context testing (Figure 2H). This second CFC protocol was designed without spaced learning sessions; however, several studies suggest that sleep plays an active role in the replay of information and memory consolidation (Dudai et al., 2015; Graves et al., 2003; Rauchs et al., 2011). In this sense, acquisition followed by consolidation can be viewed as spaced stimulation. Importantly, the freezing time in the conditioned context, CC+, was significantly less 24 h after conditioning in the $NT^{-/-}$ mice (31.9 ± 3.2 % vs. 50.5 ± 4.7 %; $p = 0.005$; Figure 2I), suggesting that NT deficiency impairs the formation and/or retrieval of contextual fear memory. As in spaced CFC, both genotypes similarly decreased their freezing levels after the fear extinction protocol, indicating that extinction of contextual fear memory was not altered by NT deficiency (Figure 2I).

Neurotrypsin is important for social interaction in juvenile mice

Next, we investigated social behavior in $NT^{-/-}$ mice. Alterations in social behavior are symptoms of several neuropsychiatric and neurological diseases. In particular, mental retardation is generally accompanied by a functional deficit in adaptive behavior, such as social skills and communication (Bieleck & Swender, 2004).

To evaluate sociability, we performed a three-chamber sociability test (Figure 3A). We observed that $NT^{-/-}$ mice spent more time near box with stimulus mouse inside (74.9 ± 10.8 s *vs.* 40.2 ± 5.7 s, $p = 0.017$; Figure 3B) compare to their control $NT^{+/+}$ littermates (153.9 ± 28.9 s vs. 34.9 ± 4.9 s, $p = 0.0029$; Figure 3B). But the $NT^{-/-}$ mice showed less preference to the stimulus mouse. This result was confirmed by the analysis of the discrimination ratio to remove individual variability in total exploration time ($NT^{-/-}$: 25.4 ± 9.6 % *vs.* $NT^{+/+}$: 55.5 ± 7.3 %, $p = 0.0267$, t-test; Figure 3C).

Age-persistent and new defects in mature neurotrypsin-deficient mice

Next, we asked if impaired CFC and sociability in juvenile $NT^{-/-}$ mice would persist after animals matured and aged and if additional defects could appear. Hence, we evaluated the behavioral phenotype of 1- to 2-year-old age-matched $NT^{-/-}$ and $NT^{+/+}$ mice in a battery of behavioral tests (Figure S2A).

In the open field test, the total distance traveled by $NT^{-/-}$ mice was not significantly different compared with $NT^{+/+}$ littermates (p = 0.355, 32.3 ± 1.6 m *vs.* 36.4 ± 3.8 m; Figure S2B). There was also no difference between genotypes in cumulative time spent in the central (p = 0.285, $NT^{-/-}$: 111.2 ± 14.6 s; $NT^{+/+}$: 134.7 ± 15.5 s) and peripheral areas (p = 0.284, $NT^{-/-}$: 488.9 ± 14.6 s; $NT^{+/+}$: 465.3 ± 15.5 s) (Figure S2C, D). Due to a slight trend for $NT^{-/-}$ mice to spend less time in the central area, the elevated plus-maze was additionally used to verify whether these mice were more anxious. However, $NT^{+/+}$ and$NT^{-/-}$ littermates spent similar amounts of time in both open arms (p = 0.827, 112.4 ± 13.8 *vs.* 108.5 ± 11.7 s) and enclosed arms (p = 0.855, 419.9 ± 16.0 s *vs.* 423.7 ± 12.7 s). There was no significant difference in discrimination ratio for the time spent in the arms (p = 0.820; $NT^{-/-}$: 57.6 ± 5.3%*;* $NT^{+/+}$: 59.2 ± 4.5%; Figure S2E-G). These results suggest that NT deficiency influences neither locomotor activity nor anxiety status.

Next, we performed a series of cognitive tests in which animals with a normal ability to memorize objects/animals during the encoding phase should spend more time exploring a new object/animal or familiar objects in a new location during the test phase in the novel object recognition test or novel object location test, respectively. In the novel object recognition test, $NT^{+/+}$ animals indeed spent more time exploring a novel object than a familiar one (p = 0.0003; 31.5 ± 2.5 s *vs.* 14.8 ± 1.5 s), whereas $NT^{-/-}$ mice spent similar amounts of time exploring novel and familiar objects (p = 0.460; 23.6 ± 2.2 *vs.* 20.4 ± 2.5 s; Figure S3A). There was a significant difference in the discrimination ratio between genotypes (p = 0.024; $NT^{-/-}$: 8.0% ± 9.1%*;* $NT^{+/+}$: 35.1% ± 6.6%; Figure S3E). In the novel object location task, $NT^{+/+}$ mice showed a tendency to explore an object with a changed spatial position during the retrieval phase (p = 0.083; 23.8 ± 2.9 *vs.* 18.2 ± 2.8 s), while $NT^{-/-}$ mice spent the same time exploring both objects (p = 0.474; 23.9 ± 1.0 s *vs.* 26.3 ± 2.7 s; Figure S3B). The difference in discrimination ratio between genotypes was close to statistical significance (p = 0.068, Mann-Whitney test; Figure S3F).

To test the ability of $NT^{-/-}$ mice to memorize the temporal sequence of events, we performed a temporal order recognition task. However, both $NT^{-/-}$ and $NT^{+/+}$ mice at this age failed to spend more time exploring the object less recently shown than they spent exploring the other object (p=0.346 and 0.799, respectively; Figure S3C). There was no difference in the discrimination ratio between genotypes (p = 0.278; $NT^{-/-}$: -15.6% ± 8.6%, $NT^{+/+}$: -2.0% ± 8.5%; Figure S3G). To test the capacity of $NT^{-/-}$miceto recognize and memorize other mice, we performed the social recognition test. Here, mice of both genotypes exhibited some preference for novel mice ($NT^{-/-}$: 12.8% ± 10.0%, $NT^{+/+}$: 18.9% ± 7.7%; Figure S3D). The exploration time that $NT^{+/+}$ animals spent around novel animals tended to be higher than the time spent around familiar animals (p = 0.053; 53.4 ± 6.2 s *vs.* 36.1 ± 4.7 s; Figure S3D, H)., Thus, aged $NT^{-/-}$ mice showed at least mild impairment in all recognition memory tasks compared to age-matched $NT^{+/+}$ mice, indicating deficits in memory formation.

In line with data obtained in juvenile mice, aged $NT^{-/-}$ mice failed in the sociability test, showing an almost equal level of interest in a “stimulus” mouse and control objects (p = 0.705; 46.6 ± 5.8 *vs.* 43.3 ± 4.4 s), whereas $NT^{+/+}$ mice spent more time engaging in social communication than object exploration (p =

0.0027; 53.5 ± 5.8 *vs.* 43.3 ± 4.4 s; Figure 4A). The discrimination ratio in this test differs significantly between genotypes (p = 0.015; KO: -1.9% ± 8.9% *vs.* $NT^{+/+}$: 25.9% ± 5.6%; Figure 4B).

On day 0 of CFC, both $NT^{-/-}$ and $NT^{+/+}$ littermates exhibited freezing less than 3% of the total time in the CC+ and CC- before foot shock (Figure 4C). Two-way repeated measures ANOVA revealed a significant increase in freezing time in CC+ immediately after foot shocks ($p_{context} < 0.001$, $F_{(1,19)} = 32.728$; Figure 4D) with no difference between genotypes ($p_{genotype} = 0.899$, $F_{(1,19)} = 0.017$; $p_{context \times genotype} = 0.530$, $F_{(1,19)} = 0.409$; Figure 4D). Thus, $NT^{-/-}$ mice perceived the unconditioned stimulus and had the same ability as $NT^{+/+}$ mice to form and express fear memory. On day 1, fear memory was evaluated in a recall session. As shown in Figure 4F, animals spent more time freezing in the CC+ than in the CC- ($p_{context} < 0.001$, $F_{(1,19)} = 69.398$), as revealed by the Holm-Sidak post hoc test within the $NT^{-/-}$ ($p < 0.001$, 47.4% ± 4.9% *vs.* 21.3% ± 2.6%) and $NT^{+/+}$ groups ($p < 0.001$, 44.3% ± 3.1% *vs.* 21.5% ± 1.8%). The discrimination ratios were not different between genotypes (p = 0.701, $NT^{-/-}$: 37.3% ± 5.7%; $NT^{+/+}$: 34.8% ± 3.3%; Figure 4H middle). Thus, after maturation, $NT^{-/-}$ and $NT^{+/+}$ mice have a similar ability to discriminate contexts and recall fear memory.

From day 2 to day 4, animals experienced 9 sessions (3x each day) in the CC+ to induce contextual fear memory extinction. Two-way repeated measures ANOVA revealed a statistically significant interaction between genotype and extinction sessions ($p_{test\ phase \times genotype} = 0.0072$, $F_{(8,152)} = 2.754$; Figure 4E); post hoc analysis indicated a significant difference between $NT^{-/-}$ and $NT^{+/+}$ mice in session 8 (p = 0.014, 30.7% ± 4.1% *vs.* 19.3% ± 3.5%) and session 9 (p = 0.014, 29.0% ± 3.9% s *vs.* 17.7 ± 2.8%). Thus, $NT^{-/-}$ mice failed to exhibit contextual fear memory extinction. On day 5, another recall test was done to evaluate animals' performance in both the CC- and CC+. Two-way repeated measures ANOVA revealed a statistically significant difference in freezing time between genotypes ($p_{genotype} = 0.005$, $F_{(1,19)} = 9.853$; Figure 4G). While $NT^{+/+}$ mice spent an almost equal amount of time freezing in the CC+ and CC- (p = 0.948, 16.4% ± 2.2% *vs.* 16.2% ± 2.2%), $NT^{-/-}$ mice still spent more time freezing in the CC+ than in the CC- (p = 0.030, 26.9% ± 2.1% *vs.* 21.1% ± 1.9%). Due to the large variance, the difference in the discrimination ratio did not reach statistical significance (p = 0.184, 12.6%± 5.0% *vs.* -4.5% ± 10.9%; Figure 4I). Nevertheless, considering all differences between genotypes on days 2-5, we conclude that $NT^{-/-}$ mice (unlike $NT^{+/+}$ mice) failed to exhibit contextual fear memory extinction.

Neurotrypsin regulates spine density in juvenile mice *in vivo*

As LTP-dependent formation of filopodia is abolished in mice lacking NT (Matsumoto-Miyai et al., 2009) and dendritic filopodia are thought to be direct precursors of new dendritic spines (Jontes & Smith, 2000; Yuste & Bonhoeffer, 2004; Ziv & Smith, 1996), we addressed the question of how NT affects spinogenesis and spine morphology in naïve conditions and upon learning. For this purpose, we crossbred NT mice with Thy1-EGFP mice, then analyzed spine density and morphology in CA1 secondary

apical dendrites (Figure 5A) in naïve conditions 24 h after contextual fear conditioning and 24 h after fear memory extinction.

The results revealed striking differences between the two genotypes. $NT^{-/-}$ mice showed significantly reduced spine density in naïve and extinction conditions compared with their control $NT^{+/+}$ littermates (two-way ANOVA: $p_{\text{condition}}$ =0.621, $F_{(2, 241)}$ = 0.478; p_{genotype} = 0.0076, $F_{(1, 241)}$ = 7.252; $p_{\text{condition x genotype}}$ = 0.0111, $F_{(2, 241)}$ = 4.590; p_{naive} = 0.0010, $p_{extinction}$ =0.0422, Holm-Sidak *post hoc* test; Figure 5B, subpanel 1). Cumulative frequency curves showed that the spine density distribution shifted towards lower values in naïve $NT^{-/-}$ mice (KS-test: p = 0.0149, Figure 5B, subpanel 2). However, no difference in cumulative frequency curves was found between genotypes after acquisition or extinction of fear conditioning (Figure 5C, Figure 5B, subpanels 3,4).

Interestingly, morphological analysis determined that the percentage of thin/filopodia-like spines was significantly reduced in $NT^{-/-}$ mice (two-way ANOVA: $p_{\text{condition}}$ = 0.101, $F_{(2, 241)}$ = 2.318; p_{genotype} < 0.001, $F_{(1, 241)}$ = 28.661; $p_{\text{condition x genotype}}$ = 0.370, $F_{(2, 241)}$ = 0.998; p_{naive} = 0.011; p_{CFC} = 0.013, $p_{\text{extinction}}$ < 0.001, Holm-Sidak *post hoc* test; Figure 5C, subplanel 4), whereas the proportion of mushroom spines was higher in this genotype than in wild-type mice (two-way ANOVA: $p_{\text{condition}}$ = 0.386, $F_{(2, 241)}$ = 0.957; p_{genotype} < 0.001, $F_{(1, 241)}$ = 48.813, $p_{\text{condition x genotype}}$ = 0.257, $F_{(2, 241)}$ = 1.365; p_{naive} = 0.005; p_{CFC} < 0.001, $p_{\text{extinction}}$ < 0.001, Holm-Sidak *post hoc* test for comparisons shown in Figure 5C, subpanel 3). In agreement with these observations, we found a statistically significant reduction in spine head size in $NT^{+/+}$ mice (two-way ANOVA: $p_{\text{condition}}$ = 0.0099, $F_{(2, 241)}$ = 4.708; p_{genotype} < 0.001, $F_{(1, 241)}$ = 26.921; $p_{\text{condition x genotype}}$ = 0.005, $F_{(2, 241)}$ = 5.402; p_{naive} < 0.001, $p_{extinction}$ <0.001, Holm-Sidak *post hoc* test). However, this reduction was not present after contextual fear conditioning (Figure 5C, subpanel 1). Regarding stubby spines, no significant differences were found between genotypes and conditions (Figure 5C, subpanel 2).

Taken together, it appeared surprising that the spine head diameter was not smaller in the control group after CFC, as in all conditions (also in CFC), the percentage of thin spines was higher in the control group and the percentage of mushroom spines was larger in the mutant group. Initially, we speculated that this could be due to mature mushroom spines in the control group being larger and more mature after CFC, thus compensating for this difference. However, we observed that the mushroom spine head size was very similar in both groups of mice (p =0.286, 0.551 (0.520, 0.613) *vs*. 0.532 (0.518, 0.573); as median (quartile 1, quartile 3), Figure S4A, C). Consequently, we measured the head diameter in the thin spines after CFC. Interestingly, we observed that the thin spines were larger and most likely more mature in $NT^{+/+}$ mice (p = 0.0003, 0.2849 ± 0.006 *vs*. 0.2579 ± 0.004; Figure S4B), suggesting that NT deficiency may specifically affect the maturation of thin/filopodia-like spines. In agreement with this, a cumulative frequency plot of spine head diameter of thin spines revealed that $NT^{-/-}$ mice had a leftward shift in the cumulative curve, indicating a reduction in the head diameter for this spine type in the mutant group of mice (Figure S4D).

Finally, we studied the learning-induced changes in spatial distribution of spines following CFC and extinction. We found that spine density linearly decreases over the length of traced dendritic branches (Figure 5D). In $NT^{+/+}$ mice this non-uniformity of spine distribution was mostly visible in naïve mice, abolished after CFC session and partially restored after extinction sessions (two-way ANOVA: $p_{\text{session x distance}} = 4.91*10^{-9}$, $F_{(2, 692)} = 19.671$; Fig 5D, subpanel 4). For $NT^{-/-}$ mice we also observed a negative correlation between spine density and spine distance to the beginning of the traced dendritic branches. Nevertheless, it was less prominent and $NT^{-/-}$ mice did not show any learning-induced modulation in the spatial distribution of spines (two-way ANOVA: $p_{\text{session x distance}} = 0.146$, $F_{(2, 709)} = 1.93$; Fig 5D, subpanel 4).

Neurotrypsin-dependent cleavage of agrin plays a major role in regulating dendritic spine formation and clustering of synapses

As agrin is the only substrate of NT identified so far and its 22 kDa cleavage fragment is critically important for activity-dependent filopodia formation (Matsumoto-Miyai et al., 2009), we addressed the question of whether agrin cleavage is responsible for the putative effects of NT deficiency. To test this hypothesis, we aimed to deliver agrin-22 in the hippocampus of $NT^{-/-}$ mice and evaluate its effect on dendritic spines. For this purpose, we designed an AAV expressing agrin-22 construct specifically in neurons. The DNA construct also included a secretion signal sequence (Aricescu et al., 2006) and the red fluorescent protein scarlet as a reporter. As a control, we used a shorter version of agrin-22, agrin-15, which was shown to act as an agrin antagonist in hippocampal and cortical cultures (Hoover et al., 2003) and in acute-slice preparations (Hilgenberg et al., 2006) (Figure S5).

We injected either pAAV-Syn-Agrin22-Scarlet (AAV-Ag22) or pAAV-Syn- Agrin15-Scarlet (AAV-Ag15) at postnatal day 7 (P7) into the hippocampus of $NT^{-/-}$ mice. Subsequently, we collected samples for spine imaging at P24 after 3 consecutive days of habituation (see Figure 6A for a general scheme of the experiment) to follow the same protocol as that used in previous spine imaging experiments. As shown in Figure 6B, injection of AAV-Ag22 increased the spine density in $NT^{-/-}$ mice to similar levels as those previously observed in their control wild-type littermates ($NT^{-/-}$ + Ag22:1.539 ± 0.050 *vs.* $NT^{+/+}$: 1.647 ± 0.051). However, there was no increase in spine density when mice were injected with AAV-Ag15 (1.299 ± 0.043). The difference between mice treated with AAV-Ag22 and AAV-Ag15 was significant ($p = 0.001$).

In addition to its effect on spine density, injection of AAV-Ag22 in $NT^{-/-}$ mice showed larger spine head size compared with AAV-Ag15 treated group ($p = 0.030$; $NT^{-/-}$ + Ag22: 0.478 (0.441, 0.515) vs. $NT^{-/-}$ + Ag15: 0.432 (0.412, 0.480) µm; as median (quartile 1, quartile 3), Figure 6C). Moreover, filopodia density was apparently slightly increased in mice injected with AAV-Ag22 compared with those injected with AAV-Ag15 (0.577 ± 0.08 *vs.* 0.437 ± 0.05), but did not reach statistical significance ($p = 0.275$, Figure 6D). Additionally, we performed analysis of the spatial density of spines, however, no difference between agrin-15 and agrin-22 injected mice was detected (two-way ANOVA: $p_{\text{agrin x distance}} = 0.408$, $F_{(2, 506)} = 0.898$).

To ensure proper injections, each hippocampal slice was imaged to detect Ag22-scarlet or Ag15-scarlet expression, and only those animals with positive expression were selected for subsequent spine analysis. Both Ag22-scarlet and Ag15-scarlet labeling were diffusely distributed over neuronal somas from the *stratum pyramidale* and showed puncta distribution in the *stratum radiatum*. Distinctly, all mice injected with AAV-Ag15 exhibited a lower intensity of “agrin puncta” in the *stratum radiatum*, presumably because of less stability, as agrin-15 is not found under physiological conditions in animals (Figure S6).

To determine whether Ag22-scarlet bound its potential neuronal receptor a3NKA (a3 Na^+/K^+ ATPase) (Hilgenberg et al., 2006), CA1 slices from brains injected with AAV-Ag22 were labeled with the a3NKA monoclonal antibody. Consistent with a previous in vitrostudy (Hilgenberg et al., 2006), we observed an extensive overlap between a3NKA and “agrin puncta” expression in the *stratum radiatum* (Figure S7A). To confirm that AAV-Ag22 was properly delivered and expressed at synaptic sites, we stained CA1 slices from brains injected with AAV-Ag22 with the excitatory presynaptic marker VGLUT1. Colocalization of scarlet-tagged Ag22 and immunostained VGLUT1 confirmed that agrin-22 was concentrated at synapses (Figure S7B). Altogether, these observations provide strong evidence that virally expressed agrin-22 is properly delivered to synaptic sites in the *stratum radiatum* and overlaps with its physiological neuronal receptor a3NKA.

Next, we investigated the effect of Ag22-scarlet on VGLUT1 puncta. Interestingly, we observed that VGLUT1-positive presynapses colocalizing with Ag22-scarlet were significantly larger than those without Ag22 scarlet colocalization (0.512 ± 0.027 mm^2 *vs*. 0.120 ± 0.019 mm^2; $p < 0.0001$; Figure 7A-C). In agreement with this, a cumulative frequency plot of VGLUT1-immunopositive puncta area revealed that the presynapses colocalizing with Ag22-scarlet had a rightward shift in the cumulative curve, indicating an enlargement of VLGUT1 presynapses colocalizing with Ag22-scarlet (Figure 7D). This striking observation suggests that Ag22-scarlet may induce synapse formation or aggregation of VGLUT1-positive synaptic vesicles at presynapses.

Finally, to examine whether these large structures are composed of pre- but also postsynaptic specializations, we stained CA1 slices from brains injected with AAV-Ag22 with the excitatory presynaptic marker VGLUT1 and the excitatory postsynaptic marker PSD95. Interestingly, we observed complex synapses with multiple postsynaptic densities contacting agrin-22 clusters (see the magnification in the upper-right corner of Figure S8).

Discussion

Altogether, our results demonstrate an important role of NT in functional synaptic plasticity in different types of learning and memory and sociability in juvenile and mature mice. Moreover, we highlight the impact of NT-dependent cleavage of agrin in regulating dendritic spine formation and morphology and its potential impact on the clustering of synapses.

It has been previously reported that the level of theta-burst stimulation-induced LTP is normal in acute hippocampal slices from young $NT^{-/-}$ mice. One of the most striking phenotypes in these mice was the lack of formation of dendritic filopodia after induction of cLTP, which are very likely to be precursors of newly formed synapses (Matsumoto-Miyai et al., 2009). However, the conventional LTP protocol may not be suitable to reveal an increase in synaptic transmission due to the formation of new spines, as nascent spines are mostly silent (i.e., they lack AMPA receptors) (Durand et al., 1996; Isaac et al., 1995; Liao et al., 1995; O'Brien et al., 1999). Krámar and colleagues reported that a second TBS (TBS2) administered at least 60 min after the first TBS (TBS1) doubled the level of LTP and induced actin polymerization in more synapses compared to TBS1, supporting the idea that a new population of synapses was potentiated by TBS2 (Kramár et al., 2012). The time interval of at least 60 min was crucial to induce an additional LTP, suggesting that this time interval is necessary for the recruitment of postsynaptic density components to nascent synapses; this process can be used as a scaffold for the recruitment of NMDA and AMPA receptors. As this spaced form of LTP induced by two 1-h spaced TBSs relies on filopodia generation and their conversion into functional synapses (Kramár et al., 2012), we hypothesized that it might be affected in $NT^{-/-}$ mice. Hence, following the protocol from Krámar et al., 2012, we recorded LTP induced by two TBSs spaced by 1 h in CA3-CA1 synapses from $NT^{+/+}$ and $NT^{-/-}$ mouse slices. Our extracellular recordings revealed that $NT^{-/-}$ mice show no additional potentiation after TBS2, unlike $NT^{+/+}$ mice, suggesting that a new population of synapses induced by NT-agrin signaling could be potentiated by TBS2.

Previous studies have associated a selective impairment of LTP induced by strong stimuli at CA3-CA1 synapses with a deficit in CFC or context discrimination (Jin et al., 2013; Kochlamazashvili et al., 2010). More recent studies have also described similar combinations of impairment of context discrimination and altered LTP in the CA1 region (Darcy et al., 2014; Minge et al., 2017). Moreover, one study that linked cognitive deficits during acute neuroinflammation also supported that the CA1 region is involved in context discrimination (Czerniawski & Guzowski, 2014). Both hippocampal and amygdaloid NMDA receptors are involved in the acquisition of Pavlovian fear conditioning. This research implicates NMDA receptor-dependent LTP in these brain areas in the acquisition of conditional fear. Moreover, several studies have used a correlational approach to assess the role of hippocampal LTP in contextual fear conditioning, suggesting that hippocampal NMDA receptor-dependent LTP is required in encoding contextual representations (reviewed in Maren, 2001). Interestingly, NT activation is an NMDA receptor-dependent process (Matsumoto-Miyai et al., 2009). Hence, this prompted the question of whether NT may play a role in the acquisition of contextual fear memory.

Our "spaced" contextual fear conditioning protocol revealed that NT deficiency did not impair the retrieval of contextual memory during memory recall at d2 (48 h after the training session). However, $NT^{-/-}$ mice appeared to be less efficient in discriminating between contexts during the retrieval of fear memory. Combined results indicate that there may be significant redundancy in the neuroanatomical regions and compensatory mechanisms mediating fear conditioning (Curzon et al., 2009). This is not surprising, as the ability to store fear memories from frightening experiences accurately and reliably is essential to

survive in an ever-changing and potentially dangerous environment. This may partly justify why the loss of NT is not sufficient to result in an impairment of encoding and/or recalling of fear mnemonic processes. Another possibility to consider is the generalization effect of the context. The generalization of fear conditioning is manifested as a loss of stimulus specificity and as the emotional sensitization of associative components of memory; the generalization of fear conditioning thus leads to diminished signal discrimination and generalized anxiety (Ciocchi et al., 2010; Laxmi et al., 2003). Therefore, the more the signal is generalized, the less discrimination occurs. Previous findings indicate that fear generalization is broadly tuned and sensitive to the intensity of unconditioned stimuli (Dunsmoor et al., 2009). Indeed, it was shown that increasing foot-shock intensity (Baldi et al., 2004; Dunsmoor et al., 2009) and the number of foot shocks (Poulos et al., 2016) led to context memory generalization. Consequently, we performed a milder contextual fear conditioning protocol with one single context. The results obtained indicate that the $NT^{-/-}$ mice freeze significantly less in the conditioned context 24 h after conditioning, suggesting that the NT null mutation impairs the formation or retrieval of contextual fear memory. Importantly, NT deficiency affected neither the level of freezing before fear conditioning (normal freezing level during fully unconstrained exploration of a novel environment is 5–10% in mice) nor the significant elevation of freezing between three unconditioned stimuli, indicating that differences between genotypes at the memory recall session are not due to distinct perception of the aversive stimulus or higher basal anxiety levels. On the other hand, both genotypes similarly reduced their freezing levels after fear memory extinction, demonstrating that the extinction of contextual fear memory was not altered by NT deficiency.

Blaeser and colleagues (2006) presented a study in a mouse with a mutation in the CaM kinase isoform (CaMKK), an upstream component of the Ca^{2+}/calmodulin kinase (CaMK) cascade that has been implicated in neuronal gene transcription, synaptic plasticity, and long-term memory consolidation. Interestingly, they showed that CaMKK mutants showed normal long-term spatial memory formation and cued fear conditioning but failed to demonstrate contextual fear conditioning. In addition, they exhibited impaired activation of the downstream kinase CaMKIV/Gr and its substrate, the transcription factor cyclic AMP-responsive element-binding protein (CREB), upon fear conditioning. Similar to our juvenile NT knockout mice, these mutants exhibited normal levels of anxiety-like behavior and no deficit at all in the extinction of the freezing response (Blaeser et al., 2006). Interestingly, it was previously described that activation of the agrin receptor in neurons resulted in a tyrosine kinase-dependent increase in intracellular Ca^{2+} that engages both CaMKII and MAPK signaling pathways (Hilgenberg & Smith, 2004). Moreover, CREB phosphorylation was markedly decreased in the neurons of $NT^{-/-}$ mice after a spatial learning task and social interaction compared to hippocampal neurons of their $NT^{+/+}$ littermates (Mitsui et al., 2009), suggesting that the mechanisms downstream of the agrin receptor in neurons may be involved in this signaling pathway.

Alterations in social behavior are symptoms of several neuropsychiatric and neurological diseases. In particular, mental retardation is generally accompanied by a functional deficit in adaptive behaviors, such as using social skills and engaging in communication (Bieleck & Swender, 2004). Social interaction was

tested using the three-chamber sociability test, a widely used test paradigm to quantitatively measure this behavior (Moy et al., 2004). We found that although juvenile $NT^{-/-}$ and $NT^{+/+}$ mice stayed near the cage with the stimulus mouse significantly longer than they stayed near the empty cage, $NT^{-/-}$ mice have a remarkably lower preference and, hence, lower sociability levels compared with their control wild-type littermates. Older $NT^{-/-}$ mice showed no preference for animated objects. This outcome is different from the results of a previous study in adult (14-20-week-old) NT knockout mice in which both $NT^{-/-}$ and $NT^{+/+}$ mice sniffed the stimulus mouse for significantly longer equal time intervals than they sniffed the empty cage (Mitsui et al., 2009). Surprisingly, although normal in terms of sociability and social memory, adult NT knockout mice showed markedly reduced CREB phosphorylation in hippocampal CA1 neurons after social interaction compared to their wild-type littermates (Mitsui et al., 2009). However, CREB analysis was not performed in that work in the same animals that underwent the three-chamber sociability test. Mice that were tested for behavioral analysis were housed in single cages at least 1 week before starting the task. On the other hand, brain slices for CREB analysis came from animals that were group-housed at least 2 weeks before the test. In addition, Mitsui and colleagues (2009) used a different NT knockout model for their experiments, in which exon 1 of the PRSS12 gene (the gene encoding NT) was replaced (Mitsui et al., 2009), while in our NT knockout mouse model, part of exons 10 and 11 was replaced, resulting in a truncated NT gene lacking the region encoding the proteolytic domain (Stephan et al., 2008). In addition, the age difference may be essential, resembling the age-dependent phenotype of mice deficient in the cell adhesion molecule CHL1, which showed impaired LTP in juvenile mice, normal LTP in 2-month-old adult mice and impaired LTP at the age of 9 months (Schmalbach et al., 2015).

A direct comparison of phenotypes of juvenile and aged $NT^{-/-}$ mice also revealed several differences in their performance: 1) in fear conditioning, which was impaired in juvenile mice but normal in aged ones; 2) in fear extinction, which was normal in juvenile and impaired in aged mice; and 3) in the novel object recognition test outcomes, which were also normal in juvenile and impaired in aged mice (Table S1). Additionally, a previous analysis of adult $NT^{-/-}$ mice did not reveal significant deficits in the Morris water maze, passive avoidance, or Y-maze tests (Mitsui et al., 2009). Thus, NT deficiency shows a complex pattern of interaction with age, so some defects could be compensated for in young mice but become detectable with aging. Of note, plasticity mechanisms can undergo profound changes during aging, as has been shown, e.g., for ocular dominance plasticity (Espinosa & Stryker, 2012). This results in sensitive or critical periods of development that affect maturation of the sensory system but also fear learning and memory (King et al., 2014) and may account for the differential outcome of behavioral experiments with $NT^{-/-}$ mice between the ages.

As LTP-dependent formation of filopodia appeared to be abolished in mice lacking NT (Matsumoto-Miyai et al., 2009) and dendritic filopodia are thought to be direct precursors of new dendritic spines (Jontes & Smith, 2000; Yuste & Bonhoeffer, 2004; Ziv & Smith, 1996), we hypothesized that NT-dependent mechanisms may affect spinogenesis and/or spine morphology. As NT is released in an activity-dependent manner (Frischknecht et al., 2008), we investigated dendritic spines in both naïve mice and mice after they performed learning tasks. To assess learning-induced spine formation, we selected the

contextual fear conditioning task for two reasons. On the one hand, we found that $NT^{-/-}$ mice were impaired in the formation or retrieval of CFC, as they have significantly lower freezing levels at memory recall. On the other hand, several studies have provided evidence that FC leads to changes in spine density and/or morphology, which makes that paradigm suitable for our purpose (Abate et al., 2018; Bender et al., 2018; Giachero et al., 2013, 2015; Lai et al., 2012; Petsophonsakul et al., 2017; Pignataro et al., 2013).

We observed significantly reduced spine density in CA1 secondary apical neurons under naïve conditions in $NT^{-/-}$ mice compared to their control wild-type littermates. This is in line with a previous study describing that a different knockout model of NT had reduced spine density in neurons from the CA1 region of the hippocampus but not from the cingulate cortex (Mitsui et al., 2009). Contrary to our expectations, no differences in spine density after acquisition or extinction of CFC (learning-dependent spinogenesis) were detected between genotypes. However, it seemed that in wild-type mice, there was a tendency to reduce spine density after the acquisition of fear memory and to increase spine density again after extinction (going back to a similar scenario like that in naïve conditions). This is in line with a study that revealed that fear conditioning increased the rate of spine elimination, whereas fear extinction increased the rate of spine formation (Lai et al., 2012). Similarly, another study reported a significant decrease in total spine density after CFC relative to home caged animals that did not undergo CFC (Sanders et al., 2012). This is consistent with a documented role of stress in decreasing spine density (Bloss et al., 2011; Chen et al., 2008). In contrast, some other studies have reported no changes in spine density after CFC (Giachero et al., 2013, 2015) or an increase in spines after CFC (Abate et al., 2018; Bender et al., 2018; Pignataro et al., 2013). The discrepancy between those studies might rely on the timing of sample collection for spine counting.

However, no spine changes were observed in juvenile $NT^{-/-}$ mice between conditions. Because fear memory is particularly important to elicit defensive responses to ensure the survival of species, it is not surprising that other mechanisms of structural plasticity may be involved and even compensate, partially or wholly, for an NT deficiency.

Interestingly, the morphological analysis determined that the percentage of thin/filopodia-like spines was significantly reduced in $NT^{-/-}$ mice, whereas the proportion of mushroom spines was higher in this genotype. Regarding stubby spines, no significant differences were found between the two groups. Thin spines are highly dynamic protrusions that can grow, shrink or change into other spine subtypes (reviewed by Kasai et al., 2010). In contrast, stubby and mushroom spines are less dynamic and are relatively stable (De Roo et al., 2008; Holtmaat et al., 2005). Thus, the higher percentage of thin spines in the wild-type mice likely reflects the morphological shift of spines that concurrently fulfill the need for available synaptic sites for structural plasticity.

In agreement with the observed higher proportion of thin spines in wild-type mice, we found a statistically significant reduction in spine head size in this group of mice. However, this reduction was not present after CFC. We initially thought that this enlargement of the spine head size after CFC may be due to a

difference in the mushroom spines, which might be larger and more mature in the control group after they undergo CFC and hence allow them to compensate for this difference. Accordingly, we measured the head diameter in the mushroom spines that were automatically detected by the software used for spine analysis. Surprisingly, we found that mushroom spine head sizes were similar in both groups of mice. Consequently, we evaluated the head diameter in the thin spines after CFC. Strikingly, we observed that the thin spines were larger and most likely more mature in the wild-type control group, suggesting that NT deficiency may specifically affect the maturation of thin/filopodia-like spines. Interestingly, enlargement of nascent spines was revealed to be tightly coupled to the formation and maturation of glutamatergic synapses (Zito et al., 2009).

As agrin is the only substrate of NT identified so far and is critically important for activity-dependent filopodia formation (Matsumoto-Miyai et al., 2009), we examined whether agrin cleavage may be responsible for the observed spine loss in $NT^{-/-}$ mice. Interestingly, previous research described that the transmembrane isoform of agrin regulates dendritic filopodia (Mccroskery et al., 2009; McCroskery et al., 2006) and synapse formation (Mccroskery et al., 2009) in rat mature hippocampal neurons. Another study on agrin function in the CNS indicated that clustering of agrin using anti-agrin antibodies stimulated filopodia formation in mouse hippocampal neuronal culture (Annies et al., 2005). We investigated whether we could rescue the spine loss present in $NT^{-/-}$ mice with an AAV expressing agrin-22. As a control, we used a shorter version of agrin-22, agrin-15, which was shown to act as an agrin antagonist in hippocampal and cortical cultures (Hoover et al., 2003) and in acute-slice preparations (Hilgenberg et al., 2006; Tidow et al., 2010). The results showed that AAV-Ag22 significantly increased spine density in $NT^{-/-}$ mice. This effect was not detected when mice were injected with AAV-Ag15, suggesting a specific effect of the product of NT-dependent agrin cleavage in the promotion of spine formation. Injection of AAV-Ag22 also increased the spine head size. The outcome of this set of experiments is in line with the previous study, which showed that the transmembrane form of agrin increased the number of dendritic spines in the external plexiform layer of the olfactory bulb. Moreover, the expression of the antagonist agrin-15 interfered with spine formation in the olfactory bulb (Burk et al., 2012).

Importantly, our data are in line with the hypothesis that Ag22 signaling relies on its neuronal receptor α3NKA (Hilgenberg et al., 2006), as we observed an extensive overlap between α3NKA and “agrin puncta” expression in the *stratum radiatum* of CA1. In addition, we confirmed that AAV-Ag22 was properly delivered and expressed at synaptic sites, as both VGLUT1 and PSD95 colocalized with Ag22-scarlet at synapses. Interestingly, we found that VGLUT1-positive puncta colocalizing with Ag22-scarlet were significantly larger than those without Ag22-scarlet colocalization. This striking observation suggests that AAV-Ag22 may induce synapse growth and/or clustering of VGLUT1-positive presynapses and PSD95-positive postsynapses. This is not surprising, as it was previously described that spine growth precedes synapse formation in the adult neocortex *in vivo* (Knott et al., 2006). In addition, De Roo and colleagues (2008) reported that new spines, upon LTP, tend to be established in clusters, providing a potential mechanism for clustered plasticity specifically upon learning (De Roo et al., 2008). Interestingly,

increased clustering of potentiated synapses was also observed in a previously discussed in vitro study by Krámar et al. (2012), which simulated spaced learning in the hippocampus (Kramár et al., 2012). More recently, several studies on the topic suggest that clusters of functionally related synapses may serve as essential memory storage units in the brain (Kastellakis et al., 2015; Kerlin et al., 2019; Winnubst & Lohmann, 2012). Further superresolution and/or electron microscopy are necessary to better understand the organization of agrin-22-induced synaptic clusters.

Overall, our results provide *in vivo* evidence of the spinogenic effects of agrin-22, the product of NT-dependent agrin cleavage, and suggest that it might be an important mechanism for synaptic plasticity and synapse formation.

Methods

Animals

All experiments and behavioral procedures were conducted in accordance with animal research ethics standards defined by German law and approved by the Ethical Committee on Animal Health and Care of the State of Saxony-Anhalt (TVA 2502-2-1159 and 42502-2-1343).

Mice constitutively lacking exons 10 and 11 from the NT gene ($NT^{-/-}$) (Reif et al., 2007) and their wild-type littermates ($NT^{+/+}$) were backcrossed to C57BL/6J mice for > 9 generations. $NT^{-/-}$ and $NT^{+/+}$ mice for experiments were obtained by mating male and female $NT^{+/-}$ mice. NT mice were kindly provided by Dr. Peter Sonderegger from the University of Zurich. Heterozygous neurotrypsin ($NT^{+/-}$) mice were crossbred with Thy1-EGFP-$M^{+/-}$ mice, which were purchased from Jackson Laboratory (www.jax.org/strain/007788). The $NT^{+/+}$/Thy1-EGFP-$M^{+/}$*and $NT^{-/-}$/Thy1-EGFP-$M^{+/}$*mice (+/$_*$ stands for +/+ or +/-) used for spine analysis were obtained by mating male and female $NT^{+/-}$/Thy1-EGFP-$M^{+/-}$ mice.

C57BL/6J, NT, Thy1-EGFP-M and NT/Thy1-EGFP-M mice were bred at the animal facility of DZNE Magdeburg. For electrophysiological experiments, we used 4-week-old $NT^{-/-}$ and $NT^{+/+}$ mice of both sexes. For behavioral experiments, we used “juvenile” (3- to 5-week-old) male littermates or a cohort of aged (11- to 24-month-old age-matched; on average, 18 months old) $NT^{-/-}$ and $NT^{+/+}$ male mice. For immunohistochemistry and spine imaging, we used 3- to 4-week-old $NT^{-/-}$/Thy1-EGFP-$M^{+/}$*and $NT^{+/+}$/Thy1-EGFP-$M^{+/}$*mice of both sexes (for spine analysis associated behavioral test (contextual fear conditioning test), data collected in male juvenile mice were presented in Fig 2i). For viral injections, we used $NT^{-/-}$/Thy1-EGFP-$M^{+/}$*P7 mice of both sexes.

Mice were kept in a reversed light-dark cycle (12:12 h, light on at 9:00 pm) with access to food and water *ad libitum* and were transferred to fresh cages weekly. All behavioral experiments were carried out during the dark phase of the cycle, i.e., when mice are active.

For behavioral and spine imaging experiments, mice were individually housed 7 days before the start of the experiments. For electrophysiological experiments, mice were housed in groups of 3-4 mice per home cage. Behavioral analysis in matured mice was performed by an experimenter blinded to group identity. After the open field test, a few juvenile mice of both genotypes were excluded from further cognitive behavioral tasks, as they were not properly habituated to the arena and showed signs of nervousness, anxiety and agitation, most likely due to their young age. The numbers of mice used for each experiment are given in the figure legends. Outliers were excluded from graphs and subsequent statistical analysis using GraphPad outlier calculator software (www.graphpad.com/quickcalcs/Grubbs1.cfm). For spine imaging experiments, mice from the same litter were randomly allocated into three experimental groups (naïve, contextual fear-conditioned, and treated for extinction). For viral injections, littermates were randomly allocated into two experimental groups (AAV-Ag15 or AAV-Ag22). Injections were performed as follows: 1 mouse was injected with AAV-Ag15, then 1 mouse was injected with AAV-Ag22 , etc. On a postnatal day 7, mice were randomly picked up by their tail from the nest.

Electrophysiological recordings in hippocampal slices

Acute hippocampal slices were prepared from 4-week-old $NT^{-/-}$ and $NT^{+/+}$ mice. Each mouse was killed by cervical dislocation, followed by decapitation. The brain was removed from the skull and transferred into ice-cold artificial cerebrospinal fluid (ACSF) saturated with carbogen (95% O_2/5% CO_2) containing (in mM) 250 sucrose, 25.6 $NaHCO_3$, 10 glucose, 4.9 KCl, 1.25 KH_2PO_4, 2 $CaCl_2$, and 2.0 $MgSO_4$ (pH = 7.3). Both hippocampi were dissected out and sliced transversally (400 µm) using a tissue chopper with a cooled stage (custom-made by LIN, Magdeburg, Germany). Slices were kept at room temperature in carbogen-bubbled ACSF (95% O_2 /5% CO_2) containing 124 mM NaCl instead of 250 mM sucrose for at least 2 h before recordings were initiated.

Recordings were performed in the same solution in a submerged chamber that was continuously superfused with carbogen-bubbled ACSF (1.2 ml/min) at 32°C. Recordings of field excitatory postsynaptic potentials (fEPSPs) were performed in CA1a and CA1c with a glass pipette filled with ACSF to activate synapses in the CA1b *stratum radiatum*. The resistance of the pipette was 1-4 MΩ. Stimulation pulses were applied to Schaffer collaterals via a monopolar, electrolytically sharpened and lacquer-coated stainless-steel electrode located approximately 300 mm closer to the CA3 subfield than to the recording electrode. Basal synaptic transmission was monitored at 0.05 Hz and collected at 3 pulses/min. The spaced LTP protocol was performed as previously described (Kramár et al., 2012). LTP was induced by applying 5xTBS with an interval of 20 s. One TBS consisted of a single train of 10 bursts (4 pulses at 100 Hz) separated by 200 ms and the width of the single pulses was 0.2 ms. To induce spaced LTP, we applied two trains of TBS (TBS1/TBS2) separated by 1 h. The stimulation strength was set to provide baseline fEPSPs with slopes of approximately 50% of the subthreshold maximum. The data were recorded at a sampling rate of 10 kHz and then filtered (0-5 kHz) and analyzed using IntraCell software (custom-made, LIN Magdeburg, Germany).

Behavioral tests

All experiments were performed under uniform illumination (30 lux, unless otherwise stated), and all behavior was video recorded using a USB video camera and analyzed using ANY-maze software (ANY-maze, version 4.99, Stoelting Co., Wood Dale, IL). All recorded movies were analyzed by a trained observer blinded to the groups.

In juvenile male mice, the following behavioral tests were performed: open field test, novel object recognition test, three-chamber sociability test, and conventional and spaced contextual fear conditioning (using two different cohorts of mice). To characterize the persistence of behavioral changes found in juvenile mice and to further extend the behavioral characterization of $NT^{-/-}$ mice, a battery of eight behavioral tests was performed using one cohort of aged male mice. The test battery included the open field test, novel object location test, novel object recognition test, temporal order recognition test, three-chamber sociability test, three-chamber social recognition test, elevated plus maze test and contextual fear conditioning (CFC). The order of the tests was optimized according to the degree of invasiveness to reduce the chance that prior tests would influence animal performance in later tests (You et al., 2019). Because the cohort of matured mice included mice of varying age, covariance analysis with age as a covariate was performed for all behavioral tests. Because no effect of age was revealed (Suppl. Data 2), data for all ages were pooled and analyzed by ANOVA.

Open field test

The open field apparatus was made out of white polyacrylics and consisted of a white square arena (50 x 50 x 30 cm). Experimental subjects were carried to the testing room in their home cages at least 30 min before the beginning of the experiment. Mice were placed in the center of the open field and allowed to freely explore it for 10 min. In juvenile mice, the first 5 min were used for the analysis of the following behavioral parameters: time spent in the inner area (central zone, 30 x 30 cm) and in the outer area (periphery) of the open field arena, locomotor activity (total travel distance), average speed, immobility time, grooming activity (including washing or mouthing of forelimbs, hind paws, face, body and genitals) and number of defecations (number of fecal boli produced). The protocol for the open field test in matured mice was the same as that used for young mice. However, since the elevated plus maze test was performed to evaluate the anxiety status of the mice, parameters that highly depend on manual counting were not analyzed. Before the start of each session and between animals, the open field test apparatus was carefully wiped with a 70% alcohol solution.

New object location test

The test started 24 h after the open field test in matured mice. The same apparatus (50 x 50 x 30 cm) used for the open field test was used in the NOLT. Two pieces of A4 paper with stripe patterns were stuck to the upper middle area on two adjacent walls and served as landmarks. Experimental subjects were carried to the testing room in their home cages at least 30 min before the beginning of the experiment. The experiment included two phases: the encoding phase and the retrieval phase. During the encoding phase, two identical objects were placed at the adjacent corners of the central area (30 x 30 cm) of the

open field arena; one of them was close to the corner which had landmarks on both walls. During the retrieval phase, this object was moved to the adjacent corner of the central part in the open field area to have both objects in a diagonal configuration. In both phases mice were given 10 min for free exploration. In the same trial, objects were counterbalanced between mice. In different trials, different pairs of objects were used. The interval between the encoding and retrieval phases was 24 h. Before placing the next animal in the arena, the apparatus was carefully wiped with a 70% alcohol solution. The exploration time for each object was automatically counted by ANY-maze software. Exploration was considered to occur when the animal's head was at a distance <2 cm from the object but excluded time intervals when the animal climbed onto the object. The discrimination ratio was calculated as [time exploring the object in a novel position - time exploring the object in a familiar position]/[time exploring the object in a novel position + time exploring the object in a familiar position] x 100%.

Novel object recognition test

The same apparatus used for the open field test was used in the novel object recognition test. Experimental subjects were carried to the testing room in their home cages at least 30 min before the beginning of the experiment. The test was performed using a standard protocol (Leger et al., 2013) that included two phases: a familiarization/encoding (F) phase and a test/retrieval (R) phase. Juvenile mice were habituated to the apparatus 2 days before familiarization for 10 min each day. In matured mice, the test started 24 h after the novel location recognition test, which served as the encoding phase of the novel object recognition test. During familiarization, mice were placed in the arena for 10 min and were allowed to freely explore two identical objects separated by 25 cm in the center of the arena. During the retrieval phase, one familiar object and one novel object were placed in the center of the arena and mice were allowed to explore the apparatus for 10 min. In the same trial, objects were counterbalanced between mice; between trials, different sets of objects were used. The interval between the encoding and retrieval phases was 24 h. Before the start of each session and prior to bringing the next animal into the arena, the apparatus was carefully wiped with a 70% alcohol solution. The exploration time for each object and the total exploration time were manually estimated. Exploration was considered to have occurred when the orientation of the animal's nose was at a distance <2 cm from the object and included the time spent sniffing and directly touching the object. Novelty detection was evaluated by calculating the discrimination ratio as follows: [novel object time – familiar object time]/[novel object time + familiar object time] x 100%.

Temporal order recognition test

Matured mice were evaluated by the temporal order recognition test. The test was initiated 24 h after the novel object recognition test using the same test chamber and location of objects. This test included two encoding phases and a retrieval phase. In each encoding phase, a pair of novel identical objects were introduced to animals; in the retrieval phase, one object from each pair was used to test if animals could recognize the temporal order of objects. Objects and the relative position of objects did not change in the retrieval phase and were counterbalanced for animal genotype. The interval between any two consecutive

test phases was 1.5 h. In all three phases, animals were given 10 min for free exploration. The same criteria as in NOLT that were used to define exploration time were applied for automatic analysis by ANY-maze software. The discrimination ratio was calculated as [exploration time of the object less recently shown – exploration time of the object recently shown]/[exploration time of the object less recently shown + exploration time of the object recently shown] x 100%.

Sociability test

Sociability levels were assessed using a three-chamber apparatus (60 x 30 x 30 cm) made out of white polyacrylics and that had connecting doors between chambers. The test in juvenile mice was performed using a standard protocol (Kaidanovich-Beilin et al., 2011): mice were habituated to the apparatus 2 h before the test for 10 min. Subsequently, one “stimulus” mouse was placed inside a small cage at one end of the compartments and an identical empty cage was placed in the opposite compartment. The mouse performing the test was allowed to explore the whole apparatus for 10 min. The exploration times spent near the cage containing the stimulus mouse and near the empty cage were estimated. The time spent sniffing and directly touching the mouse and the empty cage was considered as exploration time. In juvenile mice, as active social interaction is difficult to track automatically and hard to distinguish from time spent merely in proximity to the social partner, social interaction was analyzed and scored manually by an experimenter who was blind to the mouse genotype. In the three-chamber sociability test, the discrimination ratio was calculated as follows: [stimulus mouse time – empty cage time]/[stimulus mouse time + empty cage time] x 100%. Before the start of each session and before placing the next animal into the apparatus, the three-chamber sociability test apparatus was carefully wiped with a 70% alcohol solution; stimulus mice were changed every two sessions to avoid anxiety and stress.

In matured mice, the sociability test was initiated 24 h after the temporal order recognition test. The protocol was similar to that used for young mice. A few settings were optimized to improve the quality and reliability of automatic analysis: 1) the identical small cages that would be used as a potential container of “stimulus animals" were set on both terminal compartments in the phase when an animal was allowed to familiarize itself with the whole test environment (to reduce the exploration triggered by small cages); 2) during the test phase, a novel object was put into the small cage which had no animal inside as a stimulus (to better control the preference of subject mice for alive mice than for a nonanimated object); 3) a novel stimulus mouse was introduced after every 4 consecutive trials (to maintain the mental status of stimulus mice); and 4) the small cages were covered from above (to reduce the chance that the ANY-maze software might mistakenly track stimulus mouse movement rather than subject mouse movement, leading to the creation of an artifact). After these optimizations, the automatic analysis was precise enough to track the movements of subject mice and reflect their interests in other animals. Exploration was considered to have occurred when the orientation of the animal’s head was at a distance <2 cm from the cages but excluded instances when the animal climbed onto the small cages.

Social recognition test

The test was performed in matured mice in the three-chamber maze and was initiated 4 h after the sociability test using similar basic settings. The familiar stimulus mouse was placed inside the same small cage at the same end of the compartments as in the sociability test, and a novel stimulus mouse was placed inside the opposite compartment. Mice performing the test were given 10 min to freely explore the three-chamber apparatus. Before placing the next subject animal in the apparatus, the apparatus was carefully wiped with a 70% alcohol solution. Stimulus animals were changed every 4 consecutive trials. The exploration time towards cages including novel or familiar stimulus animals was automatically measured by ANY-maze software using the same criteria as was used in the sociability test. The discrimination ratio was calculated as [time exploring the cage containing the novel stimulus animal - time exploring the cage containing the familiar stimulus animal]/[time exploring the cage containing the novel stimulus animal + time exploring the cage containing the familiar stimulus animal] x 100%.

Elevated plus maze test (EPM)

The EPM was performed on the day after SRT in matured mice. The maze consisted of four arms in the shape of a cross (length: 30 cm, width: 5 cm, and height from floor: 50 cm). Two arms were enclosed by 15.25 cm high walls and faced each other on opposite sides; the other two arms were open borders (Walf & Frye, 2007). To reduce behavioral bias introduced by the light-dark difference between open and enclosed arms, LED lamps were used to guarantee that the light was reflected from the ceiling over enclosed arms. The final light intensity readouts at the end of all four arms were 15 lux. The movement of mice was evaluated in a single 10-min session. The heads of the mice were tracked by ANY-maze software so that entry into open arms and enclosed arms could be noted. The time animals' heads were located in different arms as well as the discrimination ratio [(time in enclosed arms - time in open arms)/(time in closed arms + time in open arms) x 100%] were used to evaluate anxiety status in mice.

Spaced contextual fear conditioning (CFC)

A *spaced* contextual fear conditioning (CFC) paradigm was performed as previously described (Senkov et al., 2006) but with two conditioning sessions separated by 1 h instead of having only one session. Before CFC training, mice were handled and habituated to the experimental room, and the conditions were maintained in a home cage for 3 days for 5 min each day. During the training day (day 0, d0), CFC was performed as follows: mice were placed into a neutral context (CC-) (the freezing level during this time interval was taken as the baseline value for the CC-) for 5 min; 2 h later, mice were placed into a conditioned context (CC+) and 3x medium intensity foot shocks were applied (0.5 mA, 1 s) with an interval of 30 s. This procedure was repeated 1 h later (hence, spaced learning was employed). The protocol included 1 min exploration in the CC+ before the first shock was administered (the freezing level during this time interval was taken as the baseline value for the CC+), 30 s after the second shock, and again 30 s after the third shock. Mice were then left for additional 30 s in the CC+ before being transferred to a home cage. The CC+ was a chamber (20 × 20 × 30 cm) with a contrast black-and-white chess-like pattern on the walls and a metal grid on the floor. The neutral context (CC−) was the same chamber, but

with gray walls and a gray plastic floor. Before the start of each session and before placing the next animal in the apparatus, the fear conditioning apparatus was carefully wiped with a 75% alcohol solution (CC+) or with Meliseptol® having a different smell (CC-) to facilitate discrimination between both contexts. In juvenile mice, memory retrieval was tested at d2, and mice were placed in the CC+ for 5 min to assess the retention of contextual memory. Subsequently, 9x memory extinction sessions were performed on 3 consecutive days (d5-d7, 3x sessions per day). In each session, mice were placed in the CC+ for 5 min. At d9, mice were placed in the CC+ again for 5 min (second memory retrieval), and freezing was assessed to evaluate fear memory extinction. A computerized fear conditioning system (Ugo Basile, Gemonio, Italy) was used for analysis. The total freezing time was manually calculated as the percentage of 5 min (in either of the 2 contexts, CC+ and CC-) when animals showed no movement except for breathing. The discrimination ratio was calculated as follows: [freezing time in the CC+ – freezing time in CC-]/[freezing time in the CC+ + freezing time in CC-] x 100%.

Contextual fear conditioning

Classical (nonspaced) CFC was performed as above but with the following modifications. In matured mice, CFC was performed on the day after EPM. During the training day (d0), mice experienced the CC- and CC+ for 5 min each, only once. The interval between the CC- and CC+ was 2 h. The 0.6 mA foot shock with a duration of 1 sec was administered in the CC+ at 120, 180 and 240 s with. During the first recall day (d1), mice were placed in the CC+ and CC- for 5 min to confirm the contextual fear memory. From day 2 to day 4, 9x memory extinction sessions were performed (3x sessions per day) by placing mice in the CC+ for 5 min. On the second recall day (d5), mice were placed in the CC+ and CC- for 5 min to confirm the extinction of contextual fear memory. For juvenile mice, the intensity of foot shocks was slightly lower than that administered to mature mice (0.5 mA), and no CC- was present.

Spine analysis

Sample collection, perfusion, and tissue processing

Mice were individually anesthetized with 100 mg/kg ketamine and 5 mg/kg xylazine and transcardially perfused with 0.1 M phosphate buffer solution (PBS, pH 7.4) followed by 4% formaldehyde diluted in 0.1 M phosphate buffer solution for 15 min. Brains were removed and postfixed for 24 h in 4% formaldehyde-PBS at 4°C. The brains were then transferred to a sucrose solution (1 M in 0.1 M NaH_2PO_4 buffer) until the solution had infiltrated into the whole brain (~48 h) to cryoprotect the tissue. Finally, the brains were frozen in 100% 2-methylbutane at -80°C and cryosectioned in 50-µm-thick coronal sections. Floating sections were kept in cryoprotective solution (1 part ethyl glycol, 1 part glycerin, and 2 parts PBS, pH 7.4). All sections were washed 3x in 0.1 M phosphate buffer solution (PBS, pH 7.4) for 10 min with gentle shaking. Subsequently, sections were briefly washed in bidistilled water to remove salts from PBS and mounted on SuperFrost glasses with Fluoromount (Sigma F4680).

Spine imaging and deconvolution

Images were acquired using a confocal laser-scanning microscope (LSM 700, Carl Zeiss, Germany) and Zen software (Carl Zeiss, Jena, Germany). Spine imaging was performed on segments of hippocampal CA1 secondary proximal dendrites, which express EGFP in NT/Thy1-EGFP-M mice. Z-stacks were taken using a 63x oil objective (NA = 1.4) with a Z-step of 0.21 µm and 2.6x optical zoom. The following voxel size was used: 0.0644 x 0.0644 x 0.2065 µm. Deconvolution of images was performed using Huygens deconvolution software (Scientific Volume Imaging). The images were deconvolved using the "Classic Maximum Likelihood Estimation (CMLE)" algorithm implemented in Huygens software (Scientific Volume Imaging), set with 50 iterations, a quality threshold of 0.01 and an signal-to-noise ratio value of 25. A theoretical point spread function was used.

Spine density and morphology analysis

To identify, classify, and count dendritic spines, images were morphometrically analyzed using NeuronStudio software (CNIC, Mount Sinai School of Medicine, New York, NY, USA) and a custom-written Excel worksheet template to count the parameters provided by the NeuronStudio software. The analysis was performed by an experimenter blinded to group identity. Spines along the dendrites were assessed using standard parameters for the distinction of stubby-, filopodia-like/thin-, and mushroom-type spines, as previously described (Rodriguez et al., 2008; Sigler et al., 2017). Parameters were set as suggested (Rodriguez et al., 2008). Only protrusions with a clear connection of the head of the spine to the shaft of the dendrite were counted as spines. In addition, a visual examination was also used to detect false "spine calls". This systematic approach was chosen to account for possible changes in spine distribution along dendrites.

To analyze the spatial distribution of spines, we calculated the number of spines in 10 mm-long bins over a dendritic shaft. The resulting counts were divided by the total number of spines for a given dendrite to obtain spine fraction in each spatial bin of the dendrite.

Generation of agrin-expression vectors and adeno-associated viral (AAV) particles

Full-length (GeneID: 11603) agrin constructs were obtained from Dharmacon (accession: BC150703). The DNA sequence corresponding to the 22 kDa C-terminus of agrin was used to induce spinogenesis and filopodia as previously described (Matsumoto-Miyai et al., 2009), while the 15 kDa C-terminus sequence was used as a control (Hilgenberg et al., 2006). The cDNA was amplified using primers (sequences of the primers can be found in supplementary data, Table S2) and cloned into an AAV vector where the gene was expressed under the synapsin promoter and fused at the N-terminus of the red fluorescent reporter protein scarlet (Bindels et al., 2016). To secrete agrin fragments into the extracellular environment, we additionally cloned a secretion signal sequence from the receptor protein tyrosine phosphatase sigma (RPTP-s) at the N-terminus of the agrin sequence as described previously (Aricescu et al., 2006).

AAV particles were produced as previously described (McClure et al., 2011) with minor modifications. Briefly, HEK 293T cells were transfected using the calcium phosphate method with an equimolar mixture of the expression plasmid, pHelper plasmid and RapCap plasmid DJ. After 48 h of transfection, cells were

lysed using freeze-thaw cycles and treated with benzonase at a final concentration of 50 units/ml for 1 h at 37°C. The lysate was centrifuged at 8000 g at 4°C. The supernatant was collected and filtered with a 0.2-micron filter. The filtered supernatant was passed through pre-equilibrated Hitrap Heparin columns (Cat no. 17-0406-01; Ge HealthCare Life Science), followed by a wash with wash Buffer 1 (20 mM Tris, 100 mM NaCl, pH 8.0; filtered sterile). Columns were additionally washed with wash Buffer 2 (20 mM Tris 250 mM NaCl, pH 8.0; filtered sterile). Viral particles were eluted with elution buffer (20 mM Tris 500 mM NaCl, pH 8.0; filtered sterile). Amicon Ultra-4 centrifugal filters (100 kD cutoff) were used to exchange the elution buffer with sterile PBS. Finally, viral particles were filtered through a 0.22 µm syringe filter (Sigma-Aldrich, product no. Z741696-100EA), aliquoted and stored at -80°C until required.

AAV intrahippocampal injections

$NT^{-/-}$/Thy1-EGFP-$M^{+/-}$ mice of both sexes were anesthetized at postnatal day P7 with 3% isoflurane (Baxter, Germany) delivered as a mixture with O_2 through a vaporizer (Matrx VIP 3000, Midmark, Versailles, USA) and a custom-made mouse breathing mask that was a suitable size for P7 mice. The cranial skin was locally disinfected and incised, the skull was exposed by displacement of the skin and muscles, and a small hole was drilled into the skull at the injection site. Craniotomy was performed on both hemispheres using stereotaxic information with respect to external landmarks on the skull, such as lambda and bregma and to other distinct landmarks, such as characteristic blood vessels of the bone and the brain (Xiong et al., 2017), which had to be adapted to the smaller size of the young skull and brain. The following coordinates were used to target the CA1 area: ML, 1 mm and DV, 1.2 mm. A total of 500 nl of viral suspension (1.84×10^{11} particles/ml) was injected per hemisphere using a pulled glass micropipette (World Precision Instruments, WPI, glass capillaries with product no. 4878) and a nanoliter injector (WPI, Nanoliter 2010). To prevent backflow, the micropipette was left in the brain for 5 min before it was pulled out. The scalp was closed and sutured, and then the animals were allowed to recover on a heated pad. P7 pups were separated from the mother for a maximum of 3 h to prevent them from being rejected.

Immunohistochemistry

Sample collection, animal perfusion and tissue processing were performed as described above for spine analysis. For a3NKA, VGLUT1 and PSD95 immunolabeling, 40 µm free-floating sections were washed in PBS (3x 10 min, at room temperature (RT) with gentle shaking) and incubated for 1 h (at RT with gentle shaking) in a blocking and permeabilizing solution containing 5% normal goat serum (NGS, Gibco, 16210-064), 0.5% Triton X-100 (Sigma Aldrich, T9284) and 0.1% Tween-20 (Roth, 9127.1) in PBS. Subsequently, slices were treated for 24 h (at 4°C with gentle shaking) with the primary antibody in PBS containing 5% NGS, 0.5% Triton X-100 and 0.1% Tween-20. Anti-sodium potassium ATPase alpha 3 (mouse, dilution 1:250, XVIF9-G10, Novus Biologicals), anti-VGLUT1 (guinea pig, dilution 1:1000, 135304, Synaptic Systems) and anti-PSD95 (mouse, dilution 1:500, Ab2723, Abcam) were used as primary antibodies. The slices were then washed 3x for 10 min at RT in PBS containing 0.1% Triton X-100 and 0.1% Tween-20 (washing buffer) and incubated on a shaker for 3 h at RT with the secondary antibody.

Secondary antibodies conjugated with Alexa 405 and 488 (Life Technologies) against the respective primary antibody were used with a dilution of 1:800 for Alexa 488 and 1:500 for Alexa 405). Afterward, slices were washed 3x 10 min at RT with washing buffer and 1x 10 min at RT with PBS, then mounted on SuperFrost glass with Fluoromount (Sigma F4680).

Image analysis

Images were acquired using a confocal laser-scanning microscope (LSM 700, Carl Zeiss, Germany) and Zen software (Carl Zeiss, Jena, Germany). ImageJ 1.46 software (NIH, USA) was used for image analysis. To analyze the size of VGLUT1-positive puncta colocalizing or not with Ag22-Scarlet, three independent images were selected for counting. For each image, channels were separated (Image > Color > Split channels). Then, thresholds were manually adjusted for each channel (Image > Adjust > Threshold (using Yen and Over/Under functions)). Subsequently, binary maps were created (Process > Binary > Make binary), and VGLUT1 puncta were recognized automatically as particles greater than 0.02 $pixel^2$ in the VGLUT1 channel (Analyze > Analyze particles > 0.02-Infinity). The size of each ROI was measured, and ROIs were superimposed on the binary map of the Ag22-Scarlet channel. ROIs were divided into two populations: ROIs with or without colocalization with AAV-Ag22 particles.

Statistics

Statistical analysis of the results from behavioral tests in juvenile and matured mice was performed with SigmaPlot 13.0. A normality test (Shapiro-Wilk method) and an equal variance test (Brown-Forsythe method) were applied to determine which parametric test should be used. Grubbs' test (the extreme studentized deviate method) was applied to determine whether one of the values in the list is a significant outlier from the rest. For data obtained from repeated measures, a two-way RM ANOVA with the Holm-Šidák post hoc test was applied (CFC, LTP). For data not repeatedly acquired from many groups, 2-way ANOVA with the Holm-Šidák post hoc test was applied (LTP, CFC associated spine analysis). For data collected from a single test based on novelty recognition (NOLT, NORT, TORT, Sociability, SRT), a two-sided paired t-test was applied for analysis of exploring time. For other comparisons between two groups (discrimination ratios, datasets in OF, EPM, spine analysis in rescue experiment), a two-sided unpaired t-test was applied. For comparison of datasets failed in the equal variance test (Fig.6C, Fig.6D, Fig.7D, Fig.S2B, Fig.S4A), Welch's t-test was applied. $P < 0.05$ was used to reject the null hypothesis. Linear regression followed by ANOVA analysis was used to analyse the spatial distribution of the spines. For comparison of cumulative distributions of dendritic spine parameters, the Kolmogorov-Smirnov test was used.

Declarations

Acknowledgments

We thank Peter Sonderegger for $NT^{-/-}$ mice and Carla Cangalaya for assistance with the blinding of experiments.

Funding

This work has been supported by funding from the European Union's 7 Framework Programme under Marie Curie grant agreement No. 606950, Initial Training Network EXTRABRAIN (to A.D.).

Competing interests

All authors declare no competing interests.

Author contributions

M.F.-F., S.J., O.S., R.F. and A.D. designed the study. M.F.-F. performed spine and synaptic puncta analysis and behavioral experiments in juvenile mice. S.J., S.A. performed spine spatial density analysis, O.S. and A.M. performed and analyzed behavioral experiments in aged mice. J.S. performed LTP experiments. R.K. and M.S. designed and generated viral vectors. R.F. received and initiated the breeding of $NT^{-/-}$ mice. M.F.-F., S.J., and A.D. wrote the manuscript. All authors edited the manuscript.

Data availability

The source data and statistical analyses underlying all figures are provided as Source Data files. The datasets generated during and/or analyzed during the current study are available from the corresponding author on reasonable request.

Ethics approval

This study was performed in line with the principles of the Declaration of Helsinki. Approval was granted by the Ethical Committee on Animal Health and Care of the State of Saxony-Anhalt (TVA 2502-2-1159 and 42502-2-1343).

Additional information

Supplementary information: The online version contains supplementary material. Correspondence and requests for materials should be addressed to Oleg Senkov or Alexander Dityatev.

References

1. Abate AG, Colazingari S, Conversi D, Bevilacqua A (2018) Dendritic spine density and EphrinB2 levels of hippocampal and anterior cingulate cortex neurons increase sequentially during formation of recent and remote fear memory in the mouse. Brain Res Bull 344:120–131
2. Annies M, Bittcher G, Ramseger R, Rgen J, Schinger L, Wö S, Porten E, Abraham C, Rüegg MA, Kröger S (2006) Clustering transmembrane-agrin induces filopodia-like processes on axons and dendrites. Mol Cell Neurosci 31(3):515–524. https://doi.org/10.1016/j.mcn.2005.11.005

3. Aricescu AR, Lu W, Jones EY (2006) A time- and cost-efficient system for high-level protein production in mammalian cells. Acta Crystallogr Sect D: Biol Crystallogr 62(10):1243–1250. https://doi.org/10.1107/S0907444906029799
4. Baldi E, Lorenzini CA, Bucherelli C (2004) Footshock intensity and generalization in contextual and auditory-cued fear conditioning in the rat. Neurobiol Learn Mem 81(3):162–166. https://doi.org/10.1016/j.nlm.2004.02.004
5. Bender C, Giachero M, Comas-Mutis R, Molina V, Calfa D (2018) Stress influences the dynamics of hippocampal structural remodeling associated with fear memory extinction. Neurobiol Learn Mem 155:412–421. https://doi.org/10.1111/poms.12938
6. Bieleck J, Swender S (2004) The Assessment of Social Functioning in Individuals With Mental Retardation. Behav Modif 28(5):694–708. https://doi.org/10.177/0145445503259828
7. Bindels DS, Haarbosch L, Van Weeren L, Postma M, Wiese KE, Mastop M, Aumonier S, Gotthard G, Royant A, Hink MA, Gadella TWJ (2016) MScarlet: A bright monomeric red fluorescent protein for cellular imaging. Nat Methods 14(1):53–56. https://doi.org/10.1038/nmeth.4074
8. Blaeser F, Sanders MJ, Truong N, Ko S, Wu LJ, Wozniak DF, Fanselow MS, Zhuo M, Chatila TA (2006) Long-Term Memory Deficits in Pavlovian Fear Conditioning in Ca2+/Calmodulin Kinase Kinase-Deficient Mice. Mol Cell Biol 26(23):9105–9115. https://doi.org/10.1128/MCB.01452-06
9. Bloss EB, Janssen WG, Ohm DT, Yuk FJ, Wadsworth S, Saardi KM, McEwen BS, Morrison JH (2011) Evidence for Reduced Experience-Dependent Dendritic Spine Plasticity in the Aging Prefrontal Cortex. J Neurosci 31(21):7831–7839. https://doi.org/10.1523/JNEUROSCI.0839-11.2011
10. Burk K, Desoeuvre A, Boutin C, Smith MA, Kröger S, Bosio A, Tiveron M-C, Cremer H (2012) Agrin-Signaling Is Necessary for the Integration of Newly Generated Neurons in the Adult Olfactory Bulb. J Neurosci 32(11):3759–3764. https://doi.org/10.1523/JNEUROSCI.4906-11.2012
11. Chen Y, Dube CM, Rice CJ, Baram TZ (2008) Rapid Loss of Dendritic Spines after Stress Involves Derangement of Spine Dynamics by Corticotropin-Releasing Hormone. J Neurosci 28(11):2903–2911. https://doi.org/10.1523/JNEUROSCI.0225-08.2008
12. Ciocchi S, Herry C, Grenier F, Wolff SBE, Letzkus JJ, Vlachos I, Ehrlich I, Sprengel R, Deisseroth K, Stadler MB, Müller C, Lüthi A (2010) Encoding of conditioned fear in central amygdala inhibitory circuits. Nature 468(7321):277–282. https://doi.org/10.1038/nature09559
13. Curzon P, Rustay NR, Browman KE (2009) Cued and Contextual Fear Conditioning for Rodents. Methods of Behavior Analysis in Neuroscience. Taylor & Francis Group, LLC, Second, pp 19–37
14. Czerniawski J, Guzowski JF (2014) Acute Neuroinflammation Impairs Context Discrimination Memory and Disrupts Pattern Separation Processes in Hippocampus. J Neurosci 34(37):12470–12480. https://doi.org/10.1523/JNEUROSCI.0542-14.2014
15. Darcy MJ, Jin SX, Feig LA (2014) R-Ras contributes to LTP and contextual discrimination. Neuroscience 277:334–342. https://doi.org/10.1016/j.neuroscience.2014.07.010
16. De Roo M, Klauser P, Muller D (2008) LTP promotes a selective long-term stabilization and clustering of dendritic spines. PLoS Biol 6(9):1850–1860. https://doi.org/10.1371/journal.pbio.0060219

17. Dudai Y, Karni A, Born J (2015) The Consolidation and Transformation of Memory. Neuron 88(1):20–32. https://doi.org/10.1016/j.neuron.2015.09.004
18. Dunsmoor JE, Mitroff SR, Labar KS (2009) Generalization of conditioned fear along a dimension of increasing fear intensity. Learn Mem 16(7):460–469. https://doi.org/10.1101/lm.1431609
19. Durand GM, Kovalchuk Y, Konnerth A (1996) Long-term potentiation and functional synapse induction in developing hippocampus.Nature Letters, *381*
20. Espinosa JS, Stryker MP (2012) Development and Plasticity of the Primary Visual Cortex. Neuron 75(2):230–249. https://doi.org/10.1016/j.neuron.2012.06.009
21. Ferrer-Ferrer M, Dityatev A (2018) Shaping Synapses by the Neural Extracellular Matrix. Front Neuroanat 12(May):1–16. https://doi.org/10.3389/fnana.2018.00040
22. Frischknecht R, Fejtova A, Viesti M, Stephan A, Sonderegger P (2008) Cellular/Molecular Activity-Induced Synaptic Capture and Exocytosis of the Neuronal Serine Protease Neurotrypsin. J Neurosci 28(7):1568–1579. https://doi.org/10.1523/JNEUROSCI.3398-07.2008
23. Giachero M, Calfa GD, Molina VA (2013) Hippocampal structural plasticity accompanies the resulting contextual fear memory following stress and fear conditioning. Learn Memory 20(11):611–616. https://doi.org/10.1101/lm.031724.113
24. Giachero M, Calfa GD, Molina VA (2015) Hippocampal dendritic spines remodeling and fear memory are modulated by GABAergic signaling within the basolateral amygdala complex. Hippocampus 25(5):545–555. https://doi.org/10.1002/hipo.22409
25. Graves L, Heller E, Pack A, Abel T (2003) Sleep deprivation selectively impairs memory consolidation for contextual fear conditioning. Learn Mem 10(3):168–176. https://doi.org/10.1101/lm.48803.LEARNING
26. Gschwend TP, Krueger SR, Kozlov SV, Wolfer DP, Sonderegger P (1997) Gschwend (1997). Neurotrypsin a novel multidomain serine protease expressed in the nervous system. Mol Cell Neurosci. *Molecular and Cellular Neuroscience*, *9*, 207–219
27. Harris KM (2020) Structural LTP: from synaptogenesis to regulated synapse enlargement and clustering. Curr Opin Neurobiol 63:189–197. https://doi.org/10.1016/j.conb.2020.04.009
28. Hilgenberg LGW, Smith MA (2004) Agrin signaling in cortical neurons is mediated by a tyrosine kinase-dependent increase in intracellular Ca2 + that engages both CaMKII and MAPK signal pathways. J Neurobiol 61(3):289–300. https://doi.org/10.1002/neu.20049
29. Hilgenberg LGW, Su H, Gu H, 'dowd O, Smith MA (2006) a3Na + /K + -ATPase Is a Neuronal Receptor for Agrin. Cell 125:359–369. https://doi.org/10.1016/j.cell.2006.01.052
30. Holtmaat AJGD, Trachtenberg JT, Wilbrecht L, Shepherd GM, Zhang X, Knott GW, Svoboda K (2005) Transient and persistent dendritic spines in the neocortex in vivo. Neuron 45(2):279–291. https://doi.org/10.1016/j.neuron.2005.01.003
31. Hoover CL, Hilgenberg LGW, Smith MA (2003) The COOH-terminal domain of agrin signals via a synaptic receptor in central nervous system neurons. J Cell Biol 161(5):923–932. https://doi.org/10.1083/jcb.200301013

32. Irie F, Badie-Mahdavi H, Yamaguchi Y, Thomas Südhof EC (2012) Autism-like socio-communicative deficits and stereotypies in mice lacking heparan sulfate. *PNAS*, *109*(13), 5052–5056. https://doi.org/10.1073/pnas.1117881109
33. Isaac JTR, Nicoll RA, Malenka RC (1995) Evidence for silent synapses: Implications for the expression of LTP. Neuron 15(2):427–434. https://doi.org/10.1016/0896-6273(95)90046-2
34. Jin SX, Arai J, Tian X, Kumar-Singh R, Feig LA (2013) Acquisition of contextual discrimination involves the appearance of a RAS-GRF1/p38 mitogen-activated protein (MAP) kinase-mediated signaling pathway that promotes long term potentiation (LTP). J Biol Chem 288(30):21703–21713. https://doi.org/10.1074/jbc.M113.471904
35. Jontes JD, Smith SJ (2000) Filopodia, spines, and the generation of synaptic diversity. Neuron 27(1):11–14. https://doi.org/10.1016/S0896-6273(00)00003-9
36. Kaidanovich-Beilin O, Lipina T, Vukobradovic I, Roder J, Woodgett JR (2011) Assessment of Social Interaction Behaviors. J Visualized Experiments 0(48):1–6. https://doi.org/10.3791/2473
37. Kasai H, Fukuda M, Watanabe S, Hayashi-Takagi A, Noguchi J (2010) Structural dynamics of dendritic spines in memory and cognition. Trends Neurosci 33(3):121–129. https://doi.org/10.1016/j.tins.2010.01.001
38. Kastellakis G, Cai DJ, Mednick SC, Silva AJ, Poirazi P (2015) Synaptic clustering within dendrites: An emerging theory of memory formation. Prog Neurobiol 126:19–35. https://doi.org/10.1016/j.pneurobio.2014.12.002
39. Kerlin A, Boaz M, Flickinger D, Maclennan BJ, Dean MB, Davis C, Spruston N, Svoboda K (2019) Functional clustering of dendritic activity during decision-making. ELife 8:1–32. https://doi.org/10.7554/eLife.46966
40. King EC, Pattwell SS, Glatt CE, Lee FS (2014) Sensitive periods in fear learning and memory. Stress 17(1):13–21. https://doi.org/10.3109/10253890.2013.796355
41. Knott GW, Holtmaat A, Wilbrecht L, Welker E, Svoboda K (2006) Spine growth precedes synapse formation in the adult neocortex in vivo. Nat Neurosci 9(9):1117–1124. https://doi.org/10.1038/nn1747
42. Kochlamazashvili G, Senkov O, Grebenyuk S, Robinson C, Xiao MF, Stummeyer K, Gerardy-Schahn R, Engel AK, Feig L, Semyanov A, Suppiramaniam V, Schachner M, Dityatev A (2010) Neural cell adhesion molecule-associated polysialic acid regulates synaptic plasticity and learning by restraining the signaling through GluN2B-containing NMDA receptors. J Neurosci 30(11):4171–4183. https://doi.org/10.1523/JNEUROSCI.5806-09.2010
43. Kramár EA, Babayan AH, Gavin CF, Cox CD, Jafari M, Gall CM, Rumbaugh G, Lynch G, & R.Thompson (2012) Synaptic evidence for the efficacy of spaced learning. PNAS 109(13):5121–5126. https://doi.org/10.1073/pnas.1120700109
44. Lai CSW, Franke TF, Gan W-B (2012) Opposite effects of fear conditioning and extinction on dendritic spine remodelling. Nature 483(7387):87–91. https://doi.org/10.1038/nature10792

45. Laxmi TR, Stork O, Pape HC (2003) Generalisation of conditioned fear and its behavioural expression in mice. Behav Brain Res 145(1–2):89–98. https://doi.org/10.1016/S0166-4328(03)00101-3
46. Leger M, Quiedeville A, Bouet V, Haelewyn B, Boulouard M, Schumann-Bard P, Freret T (2013) Object recognition test in mice. Nat Protoc 8(12):2531–2537. https://doi.org/10.1038/nprot.2013.155
47. Liao D, Hessler NA, Malinow R (1995) Activation of postsynaptically silent synapses during pairing-induced LTP in CA1 region of hippocampal slice. *Nature Letters*, *375*
48. Maren S (2001) Neurobiology of Pavlovian Fear Conditioning. Annu Rev Neurosci 24:897–931. https://doi.org/10.1146/annurev.psych.55.090902.141409
49. Matsumoto-Miyai K, Sokolowska E, Zurlinden A, Gee CE, Lüscher D, Hettwer S, Wölfel J, Ladner AP, Ster J, Gerber U, Rülicke T, Kunz B, Sonderegger P (2009) Coincident Pre- and Postsynaptic Activation Induces Dendritic Filopodia via Neurotrypsin-Dependent Agrin Cleavage. Cell 136(6):1161–1171. https://doi.org/10.1016/j.cell.2009.02.034
50. McClure C, Cole KLH, Wulff P, Klugmann M, Murray AJ (2011) Production and Titering of Recombinant Adeno-associated Viral Vectors. J Visualized Experiments 57:5–10. https://doi.org/10.3791/3348
51. Mccroskery S, Bailey A, Lin L, Daniels MP (2009) Transmembrane Agrin Regulates Dendritic Filopodia and Synapse Formation in Mature Hippocampal Neuron Cultures. Neuroscience 163(1):168–179. https://doi.org/10.1016/j.neuroscience.2009.06.012
52. McCroskery S, Chaudhry A, Lin L, Daniels MP (2006) Transmembrane agrin regulates filopodia in rat hippocampal neurons in culture. Mol Cell Neurosci 33(1):15–28. https://doi.org/10.1016/j.mcn.2006.06.004
53. Minge D, Senkov O, Kaushik R, Herde MK, Tikhobrazova O, Wulff AB, Mironov A, Van Kuppevelt TH, Oosterhof A, Kochlamazashvili G, Dityatev A, Henneberger C (2017) Heparan Sulfates Support Pyramidal Cell Excitability, Synaptic Plasticity, and Context Discrimination. Cereb Cortex 27(2):903–918. https://doi.org/10.1093/cercor/bhx003
54. Mitsui S, Osako Y, Yokoi F, Dang MT, Yuri K, Li Y, Yamaguchi N (2009) A mental retardation gene, motopsin/neurotrypsin/prss12, modulates hippocampal function and social interaction. Eur J Neurosci. https://doi.org/10.1111/j.1460-9568.2009.07029.x
55. Molinari F, Rio M, Virginia M, Férechté E-R, Augé J, Bacq D, Briault S, Vekemans M, Munnich A, Attié-Bitach T, Sonderegger P, Colleaux L (2002) Truncating Neurotrypsin Mutation in Autosomal Recessive Nonsyndromic Mental Retardation. *Science*, *298*. (5599), 1779-81
56. Moy SS, Nadler JJ, Perez A, Barbaro RP, Johns JM, Magnuson TR, Piven J, Crawley JN (2004) Sociability and preference for social novelty in five inbred strains: An approach to assess autistic-like behavior in mice. Genes Brain and Behavior 3(5):287–302. https://doi.org/10.1111/j.1601-1848.2004.00076.x
57. O'Brien RJ, Desheng X, Petralia RS, Steward O, Huganir RL, Worley P (1999) Synaptic clustering of AMPA receptors by the extracellular immediate- early gene product Narp. Neuron 23(2):309–323. https://doi.org/10.1016/S0896-6273(00)80782-5

58. Peng S, Xu J, Pelkey KA, Chandra G, Zhang Z, Bagh MB, Yuan X, Wu L-G, Mcbain CJ, Mukherjee AB (2015) Suppression of agrin-22 production and synaptic dysfunction in Cln1 À/À mice. Ann Clin Transl Neurol 2(12):1085–1104. https://doi.org/10.1002/acn3.261
59. Petralia RS, Esteban JA, Wang YX, Partridge JG, Zhao HM, Wenthold RJ, Malinow R (1999) Selective acquisition of AMPA receptors over postnatal development suggests a molecular basis for silent synapses. Nat Neurosci 2(1):31–36. https://doi.org/10.1038/4532
60. Petsophonsakul P, Richetin K, Andraini T, Roybon L, Rampon C (2017) Memory formation orchestrates the wiring of adult-born hippocampal neurons into brain circuits. Brain Struct Function 222(6):2585–2601. https://doi.org/10.1007/s00429-016-1359-x
61. Pignataro A, Middei S, Borreca A, Ammassari-Teule M (2013) Indistinguishable pattern of amygdala and hippocampus rewiring following tone or contextual fear conditioning in C57BL/6 mice. Front Behav Neurosci 7(October):1–7. https://doi.org/10.3389/fnbeh.2013.00156
62. Poulos AM, Mehta N, Lu B, Amir D, Livingston B, Santarelli A, Zhuravka I, Fanselow MS (2016) Conditioning- and time-dependent increases in context fear and generalization. Learn Memory 23(7):379–385. https://doi.org/10.1101/lm.041400.115
63. Rauchs G, Feyers D, Landeau B, Bastin C, Luxen A, Maquet P, Collette F (2011) Sleep Contributes to the Strengthening of Some Memories Over Others, Depending on Hippocampal Activity at Learning. J Neurosci 31(7):2563–2568. https://doi.org/10.1523/JNEUROSCI.3972-10.2011
64. Reif R, Sales S, Hettwer S, Dreier B, Gisler C, Wölfel J, Lüscher D, Zurlinden A, Stephan A, Ahmed S, Baici A, Ledermann B, Kunz B, Sonderegger P (2007) Specific cleavage of agrin by neurotrypsin, a synaptic protease linked to mental retardation. FASEB J 21:3468–3478. https://doi.org/10.1096/fj.07-8800com
65. Rodriguez A, Ehlenberger DB, Dickstein DL, Hof PR, Wearne SL (2008) Automated three-dimensional detection and shape classification of dendritic spines from fluorescence microscopy images. PLoS ONE 3(4). https://doi.org/10.1371/journal.pone.0001997
66. Sanders J, Cowansage K, Baumgartel K, Mayford M (2012) Elimination of Dendritic Spines with Long-Term Memory Is Specific to Active Circuits. J Neurosci 32(36):12570–12578. https://doi.org/10.1523/JNEUROSCI.1131-12.2012
67. Schmalbach B, Lepsveridze E, Djogo N, Papashvili G, Kuang F, Leshchyns'Ka I, Sytnyk V, Nikonenko AG, Dityatev A, Jakovcevski I, Schachner M (2015) Age-dependent loss of parvalbumin-expressing hippocampal interneurons in mice deficient in CHL1, a mental retardation and schizophrenia susceptibility gene. J Neurochem 135(4):830–844. https://doi.org/10.1111/jnc.13284
68. Senkov O, Sun M, Weinhold B, Gerardy-Schahn R, Schachner M, Dityatev A (2006) Polysialylated Neural Cell Adhesion Molecule Is Involved in Induction of Long-Term Potentiation and Memory Acquisition and Consolidation in a Fear-Conditioning Paradigm. J Neurosci 26(42):10888–109898. https://doi.org/10.1523/JNEUROSCI.0878-06.2006
69. Sigler A, Oh WC, Imig C, Altas B, Kawabe H, Cooper BH, Kwon HB, Rhee JS, Brose N (2017) Formation and Maintenance of Functional Spines in the Absence of Presynaptic Glutamate Release. Neuron

94(2):304–311e4. https://doi.org/10.1016/j.neuron.2017.03.029

70. Sonderegger P, Matsumoto-Miyai K (2014) Activity-controlled proteolytic cleavage at the synapse. In *Trends in Neurosciences*. https://doi.org/10.1016/j.tins.2014.05.007
71. Stephan A, Mateos JM, Kozlov SV, Cinelli P, Kistler AD, Hettwer S, Rülicke T, Streit P, Kunz B, Sonderegger P (2008) Neurotrypsin cleaves agrin locally at the synapse. FASEB J. https://doi.org/10.1096/fj.07-100008
72. Tidow H, Aperia A, Nissen P, Skou JC, Kaplan JH, Aizman O, Miyakawa-Naito A, Yuan Z, Aperia A, Kuhlbrandt W, Geering K, Lutsenko S, Kaplan JH, Garty H, Karlish SJ, Therien AG (2010) How are ion pumps and agrin signaling integrated? Trends Biochem Sci 35(12):653–659. https://doi.org/10.1016/j.tibs.2010.05.004
73. Walf AA, Frye CA (2007) The use of the elevated plus maze as an assay of anxiety-related behavior in rodents. Nat Protoc 2(2):322–328. https://doi.org/10.1038/nprot.2007.44
74. Winnubst J, Lohmann C (2012) Synaptic clustering during development and learning: the why, when, and how. Front Mol Neurosci 5(May):1–9. https://doi.org/10.3389/fnmol.2012.00070
75. Wolfer DP, Lang R, Cinelli P, Madani R, Sonderegger P (2001) Wolfer (2001). Multiple roles of neurotrypsin in tissue morphogenesis and nervous system development suggested by the mRNA expression pattern. Mol Cell Neurosci. *Molecular and Cellular Neuroscience*, *18*, 407–433
76. Xiong B, Li A, Lou Y, Chen S, Long B, Peng J, Yang Z, Xu T, Yang X, Li X, Jiang T, Luo Q, Gong H (2017) Precise Cerebral Vascular Atlas in Stereotaxic Coordinates of Whole Mouse Brain. Front Neuroanat 11(December):1–17. https://doi.org/10.3389/fnana.2017.00128
77. You R, Liu Y, Chang RCC (2019) A behavioral test battery for the repeated assessment of motor skills, mood, and cognition in mice. J Visualized Experiments 2019(145):1–10. https://doi.org/10.3791/58973
78. Yuste R, Bonhoeffer T (2004) Genesis of dendritic spines: insights from ultrastructural and imaging studies. Nat Rev Neurosci 5(1):24–34. https://doi.org/10.1038/nrn1300
79. Zito K, Scheuss V, Knott G, Hill T, Svoboda K (2009) Rapid Functional Maturation of Nascent Dendritic Spines. Neuron 61(2):247–258. https://doi.org/10.1016/j.neuron.2008.10.054
80. Ziv NE, Smith SJ (1996) Evidence for a role of dendritic filopodia in synaptogenesis and spine formation. Neuron 17(1):91–102. https://doi.org/10.1016/S0896-6273(00)80283-4

Figures

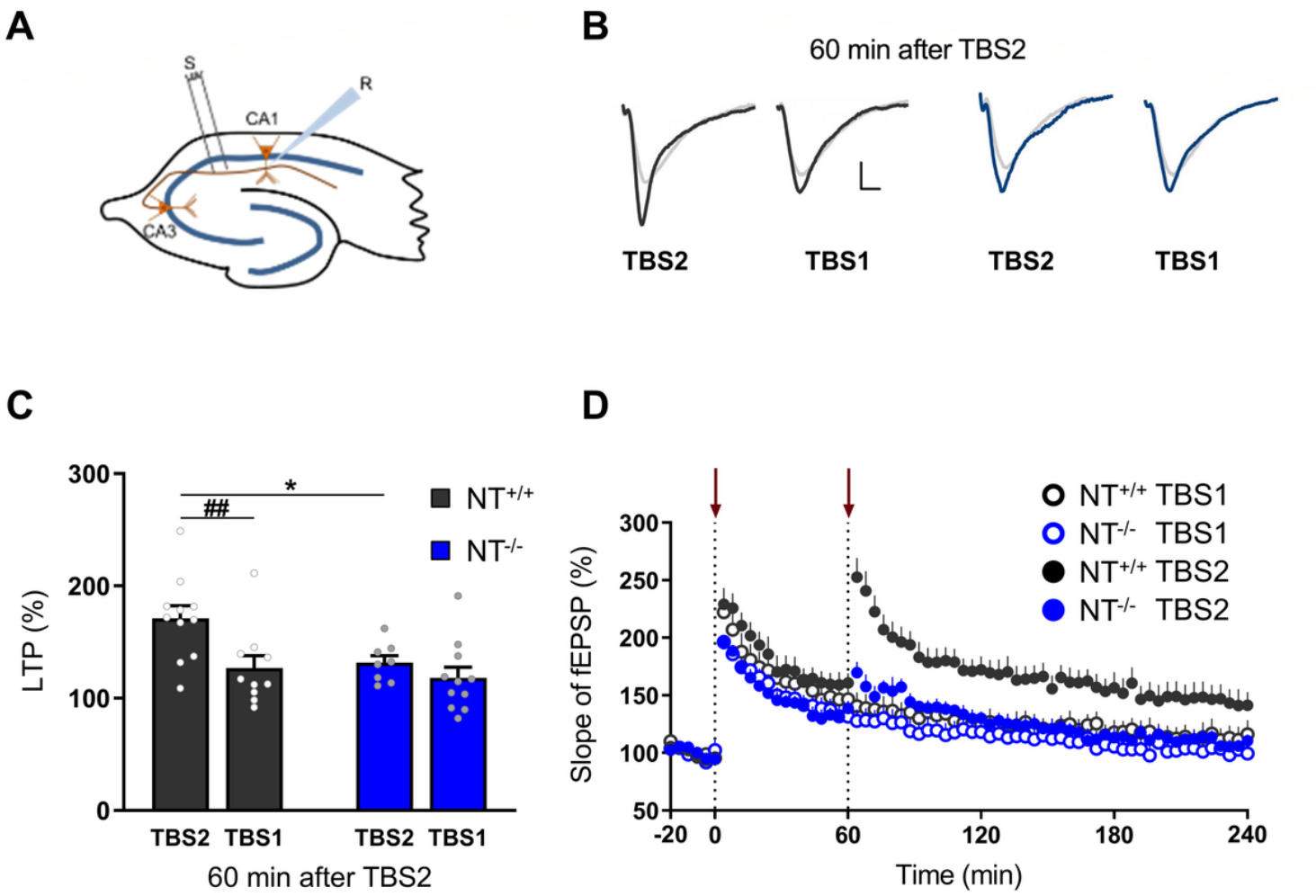

Figure 1

Spaced LTP in CA3-CA1 synapses in hippocampal slices from juvenile $NT^{-/-}$ and $NT^{+/+}$ mice. A second theta-burst stimulation train (TBS2) does not produce additional potentiation in $NT^{-/-}$ mice. (A) A schematic representation of hippocampal slices illustrating the position of both stimulating (positioned in the Schaffer collaterals) and recording (placed among apical dendrites of CA1 pyramidal cells) electrodes. (B) Representative field excitatory postsynaptic potentials (fEPSPs) from $NT^{+/+}$ (dark gray) and $NT^{-/-}$ (blue) slices, which were recorded during baseline (light gray) and 2 h after TBS1 in hippocampal slices that received either 1x TBS (TBS1) or 2x TBS (TBS2). Scale bars, 0.5 mV/2 ms. (C) A bar plot summarizing the mean LTP levels 120 min after TBS1 (60 min after TBS2). (D) Time-courses of the slope of fEPSPs show impaired spaced LTP in $NT^{-/-}$ mice. Arrows show time points when the first and second TBSs were applied. All data are shown as the mean ± SEM. The numbers of tested $NT^{+/+}$ and $NT^{-/-}$ slices/mice for each group were as follows: 11/6 ($NT^{+/+}$, 2x TBS), 10/6 ($NT^{+/+}$, 1x TBS), 8/6 ($NT^{-/-}$, 2x TBS) and 11/6 ($NT^{-/-}$, 1x TBS). Two-way ANOVA and two-way repeated-measures ANOVA with Holm-

Šidák post hoc test were applied. * $P < 0.05$, significant differences in LTP between genotypes. $^{\#\#}P < 0.01$, significant difference between LTP induced by 1x and 2x TBS in wild-type mice.

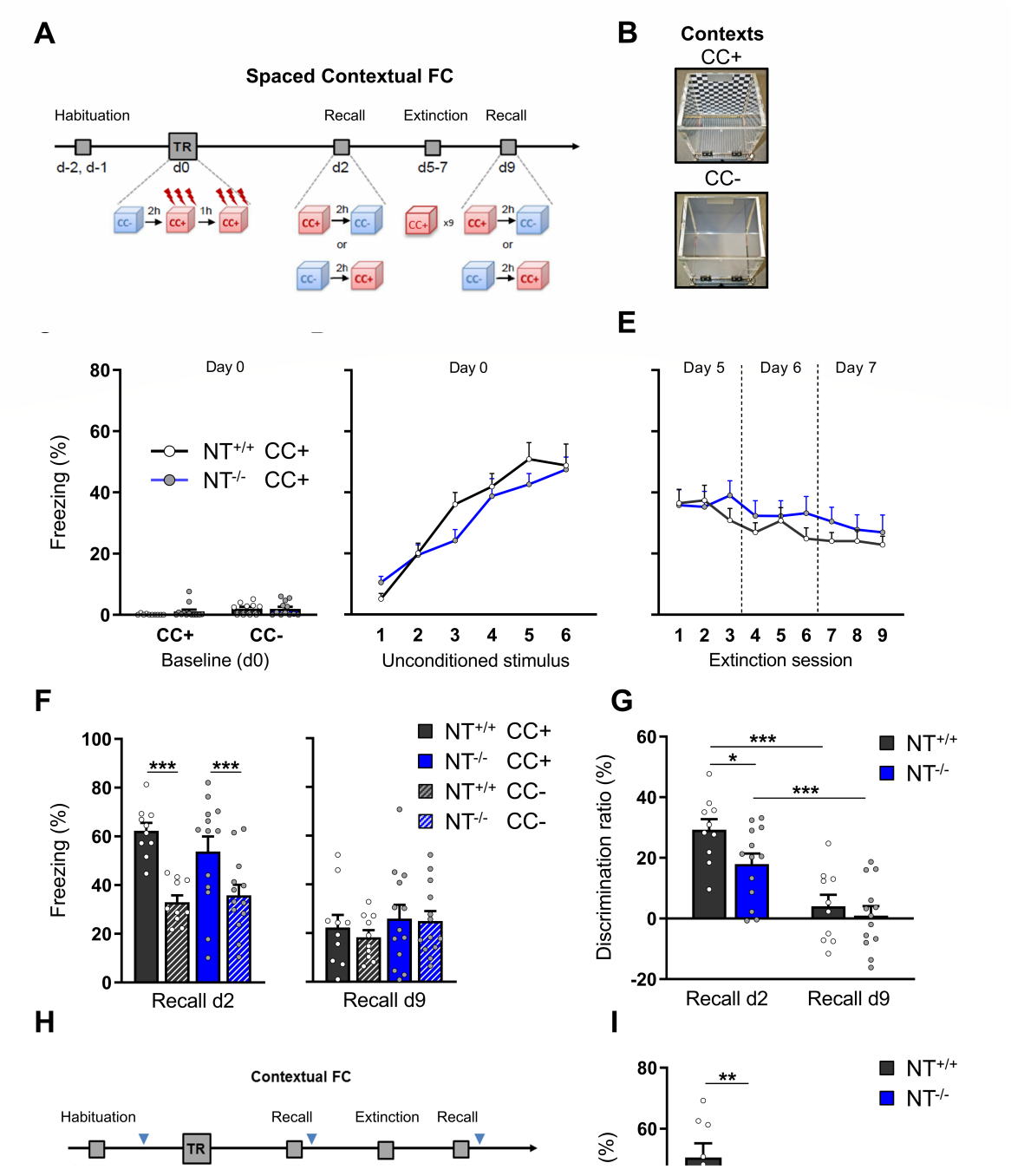

Figure 2

Contextual fear conditioning and extinction in juvenile $NT^{-/-}$ and $NT^{+/+}$ mice. $NT^{-/-}$ mice were impaired in context discrimination but not in fear memory extinction. (A) The schematic and timeline of spaced CFC. (B) Conditioned context (CC+) and neutral context (CC-). (C) Fraction of freezing in both contexts before fear conditioning (baseline). (D) Fraction of freezing in CC+ after footshocks used as unconditioned stimuli. (E) Fraction of freezing during the extinction sessions. (F) Fraction of freezing during retention of contextual fear memory revealed that both genotypes were able to distinguish between CC+ and CC- at recall on d2 and both genotypes showed extinction of fear memory on d9. (G) Analysis of the discrimination ratio revealed that the ability of $NT^{-/-}$ mice to discriminate CC+ from CC- was weaker than in $NT^{+/+}$ mice in the first recall session; after extinction, fear memory was extinguished independently of genotype. (H) The scheme and timeline of the nonspaced contextual CFC. Blue arrows indicate time points used for tissue collection for spine imaging. (I) Fraction of freezing during recalls (d1) before and (d5) after extinction. The data are shown as the mean ± SEM. $NT^{+/+}$, n = 10; $NT^{-/-}$, n = 13 in spaced CFC. $NT^{+/+}$, n = 8; $NT^{-/-}$, n = 8 in nonspaced CFC. *$P < 0.05$, **$P < 0.01$, ***$P < 0.001$. Two-way repeated-measures ANOVA with Holm-Šidák post hoc test was applied in C, D, E, F, G; nonpaired t-test was used for the panel I to compare the discrimination ratios between genotypes.

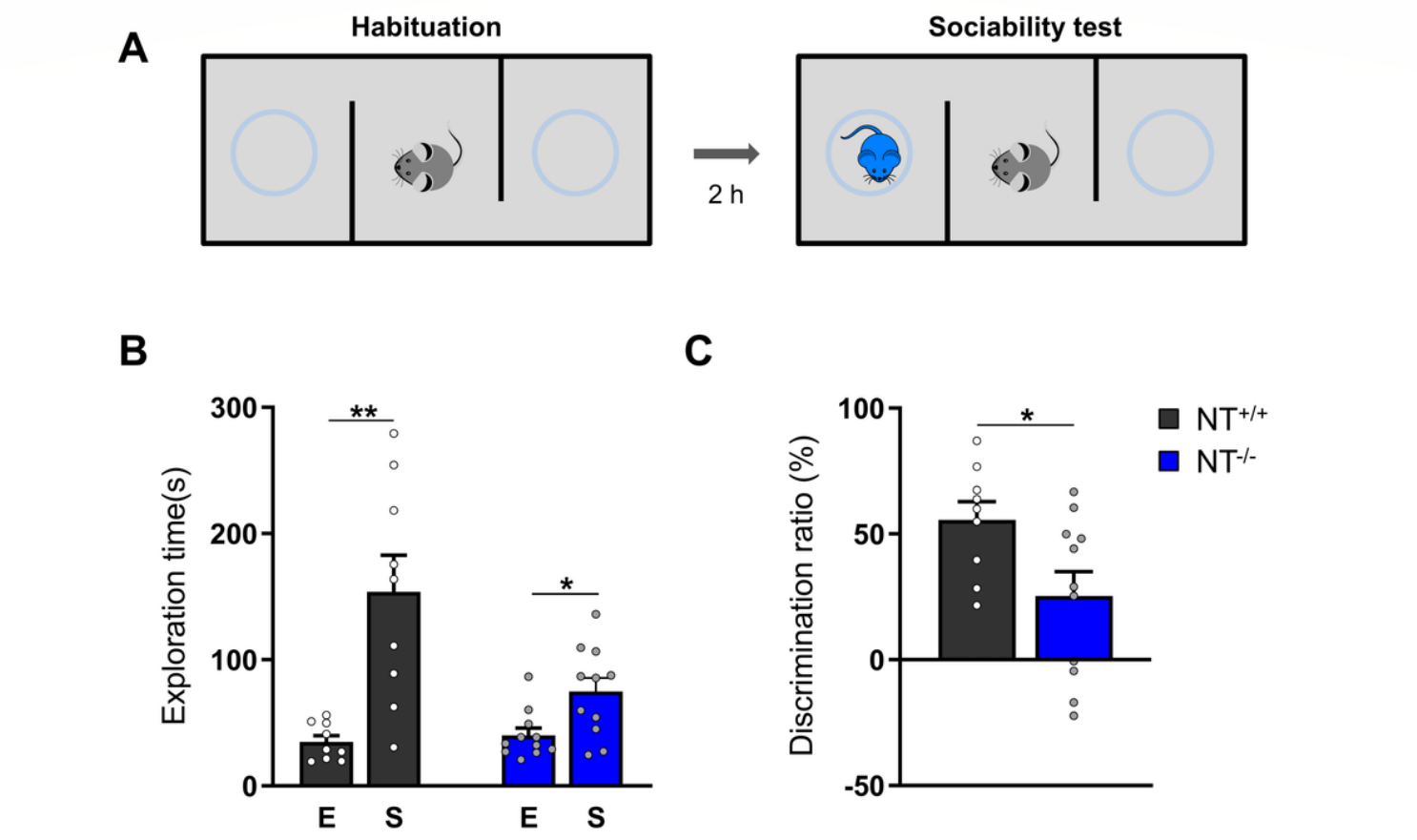

Figure 3

Juvenile NT-/- mice showed less sociability than their NT+/+ littermates in the three-chamber sociability test. (A) The timeline and schematic representation of the experimental setup. (B) The total exploration duration towards the “empty box” (E) and the “stimulus mouse” (S) during the sociability test showed that both $NT^{+/+}$ and $NT^{-/-}$ mice spent different time in E vs. S compartments (*$P < 0.05$, **$P < 0.01$, paired t-test) but $NT^{-/-}$ mice showed less preference to the stimulus mouse. (C) The discrimination index between the E and the S compartments was significantly different between the two groups of mice: *$P < 0.05$, nonpaired t-test. The data are shown as the mean ± SEM. $NT^{+/+}$: n = 9; $NT^{-/-}$: n = 11.

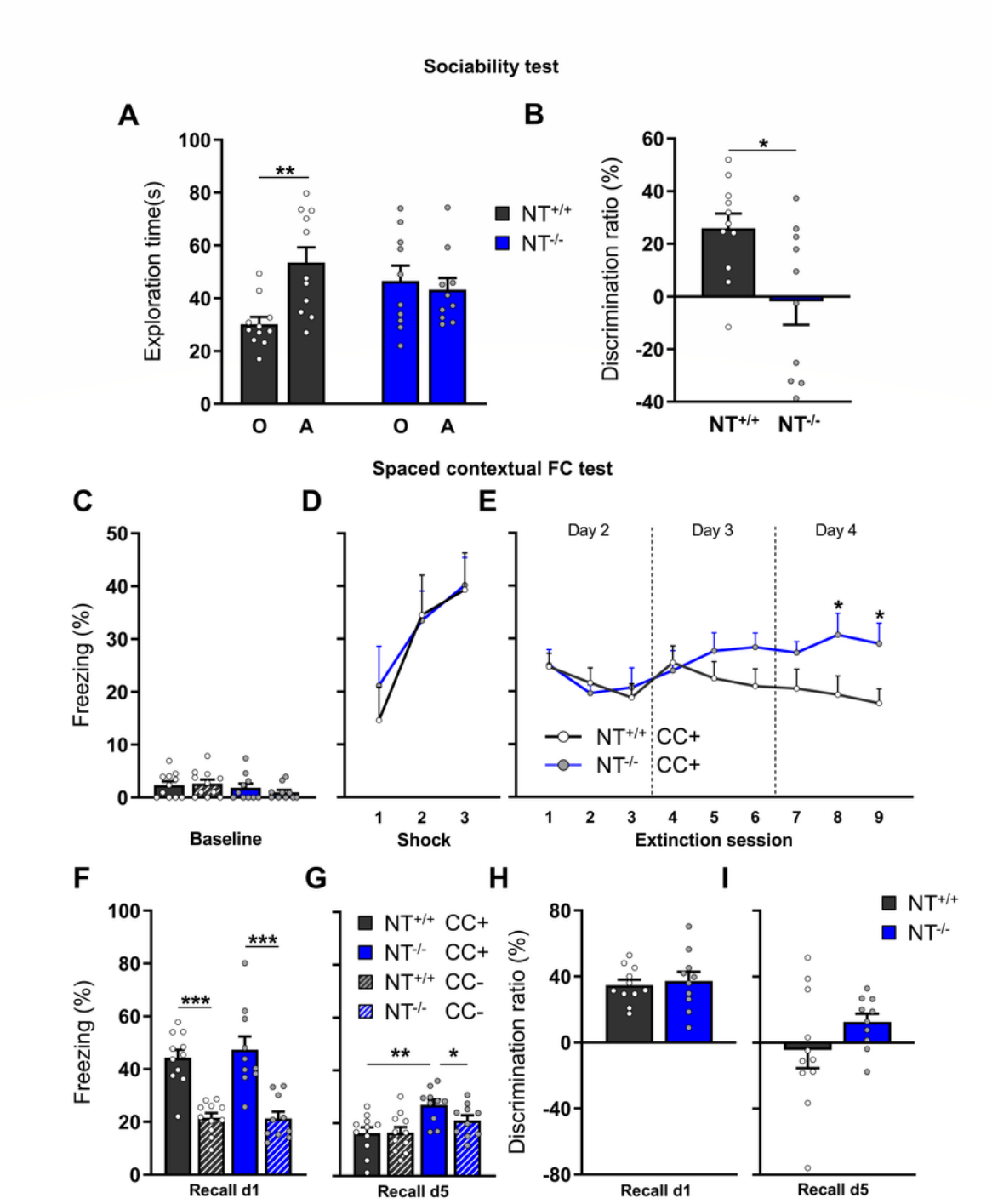

Figure 4

NT$^{-/-}$ mice showed highly significant deficits in sociability and fear memory extinction. (A) The total exploration duration towards the "object" [O] and the "stimulus animal" [A] during the sociability test. (B) The discrimination ratio between the "stimulus animal" and "object" was calculated as a fraction of exploration times for "stimulus animal" and "object". (C) Fraction of freezing duration in both contexts before fear conditioning (baseline). (D) Freezing fraction in CC+ after unconditioned stimuli (foot shocks).

(E) Freezing fraction during the extinction sessions. Percentage of freezing time in both contexts after fear conditioning. on day 1 and (F) on day 5 (G). (H, I) Discrimination ratio calculated based on freezing time during recall sessions. The data are shown as the mean ± SEM. $NT^{+/+}$: n = 11; $NT^{-/-}$: n = 10. *P < 0.05, **P < 0.01, ***P < 0.001. Two-way repeated-measures ANOVA with Holm-Šidák post hoc test was applied in C, D, E, F and G; paired t-test was applied to compare exploration time within the same group for panel A; nonpaired t-test was used in B, H and I to compare the discrimination ratios between genotypes.

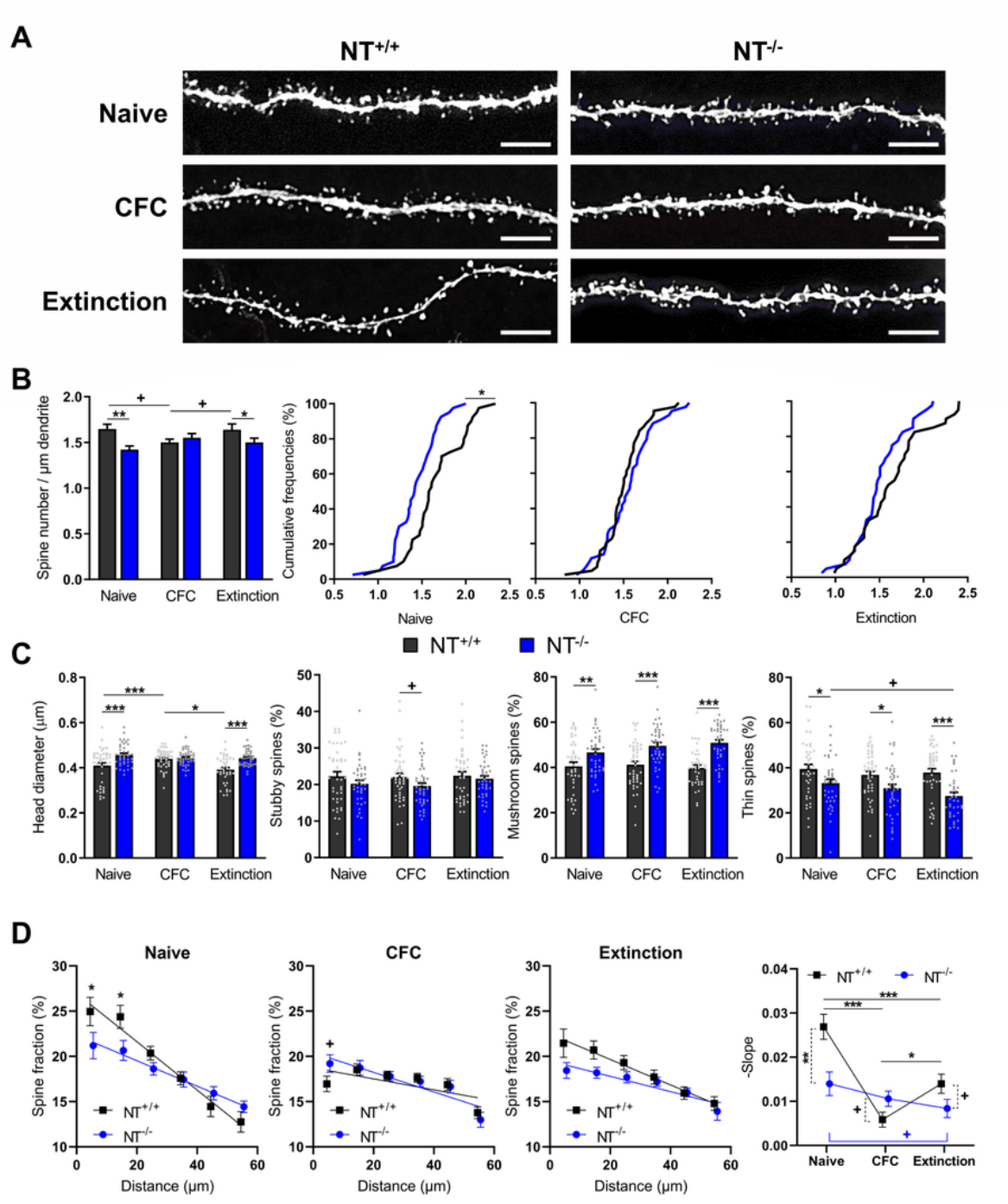

Figure 5

Blunted modulation in the number and spatial distribution of dendritic spines following CFC and extinction in NT-/- mice. (A) Representative images of CA1 secondary apical dendrites from $NT^{+/+}$ mice (left column) and their $NT^{-/-}$ littermates (right column) during different stages of CFC experiments (rows). Scale bar, 5 µm. (B) Dynamic of average and cumulative densities of spines in $NT^{+/+}$ and $NT^{-/-}$ mice

during CFC experiment. (C) Overall spine head size and spine-type composition in $NT^{+/+}$ and $NT^{-/-}$ mice during CFC experiment. (D) Comparison of spine spatial distributions evolution during CFC experiment in $NT^{+/+}$ and $NT^{-/-}$ mice (panels 1-3). Experimental data presented as means ± SEM, lines show the corresponding linear regressions. The differences in linear regression slopes and their statistical significance are shown on the right panel. The numbers of analyzed $NT^{+/+}$ and $NT^{-/-}$ dendrites/mice for each group were as follows: 40/5 ($NT^{+/+}$ naïve), 44/5 ($NT^{+/+}$ CFC), 40/5 ($NT^{+/+}$ extinction), 40/5 ($NT^{-/-}$ naïve), 43/5 ($NT^{-/-}$ CFC) and 40/5 ($NT^{-/-}$ extinction). $^{+}P < 0.1$, $^{*}P < 0.05$, $^{**}P < 0.01$, $^{***}P < 0.001$. Two-way ANOVA with Holm-Šidák post hoc test was applied in B and C; Kolmogorov-Smirnov test was used to evaluate significance for cumulative densities (B, panel 2). Standard errors and statistical significance for linear regressions were evaluated using linear regression followed by ANOVA analysis.

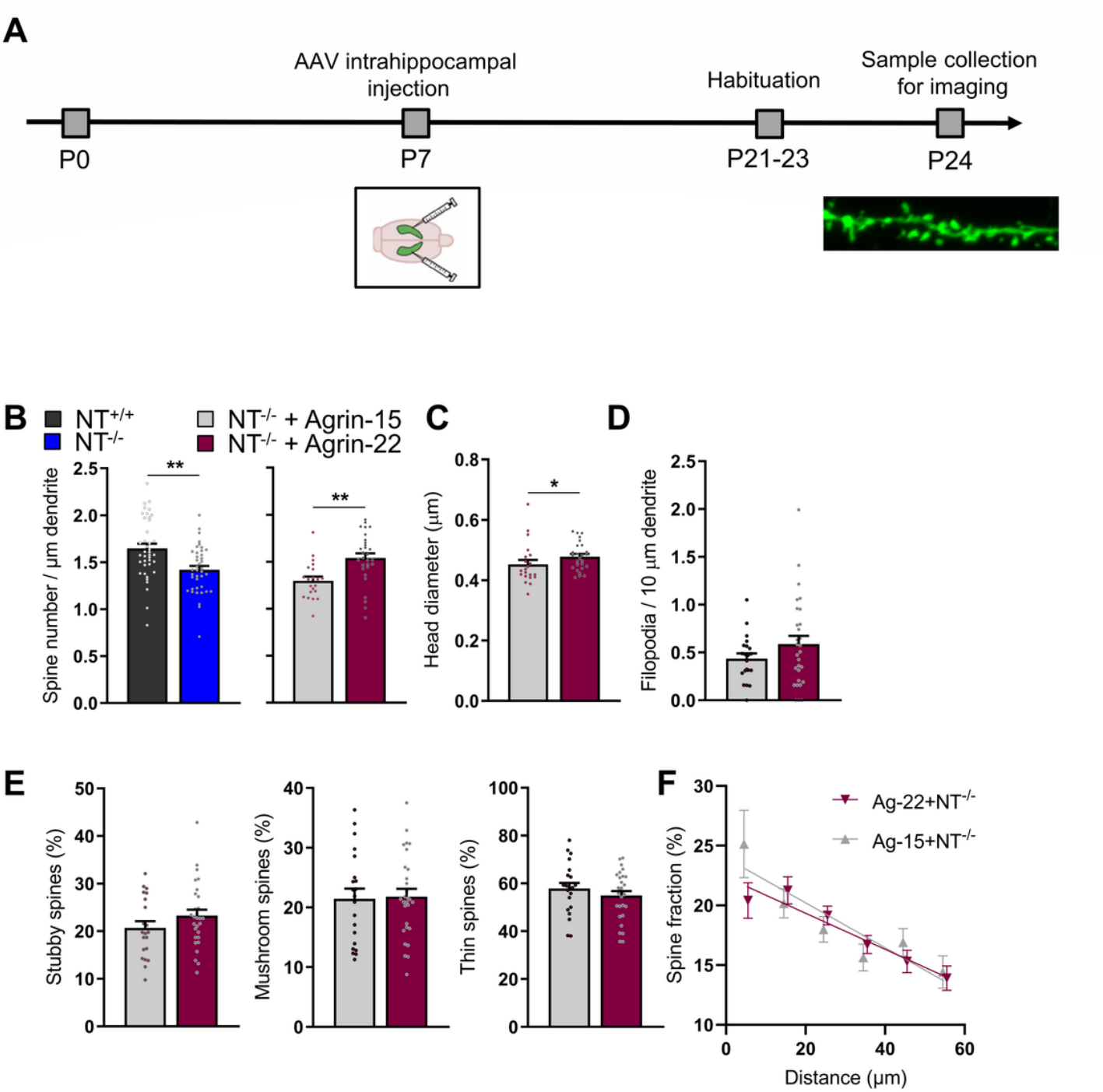

Figure 6

AAV-Ag22 restores the spine density in NT$^{-/-}$ mice to the wild-type level. (A) Schematic representation of the experiment time course. (B) Changes in spine density after injection of agrin expressing AAVs. Blue and dark gray bars show data from Figure 5B that have reference values from NT$^{-/-}$ and NT$^{+/+}$ naïve mice on the same plot. (C) Increased spine head size in AAV-Ag22 injected mice compared to AAV-Ag15 injected mice. (D) No difference between treatments in the occurrence of filopodia. (E) Spine type composition and filopodia density in naïve NT-/- mice after AAV-Ag15 or AAV-Ag22 injection. The data are presented as the mean ± SEM values per dendrite. The numbers of analyzed dendrites/mice were 29/4

(NT$^{-/-}$ injected with AAV-Ag22) and 21/3 (NT$^{-/-}$ injected with AAV-Ag15). (F) Comparison of spine spatial distributions in NT$^{-/-}$ mice after AAV-Ag15 or AAV-Ag22 injection, no difference was detected. Experimental data presented as means +/- SEM, lines show the corresponding linear regressions. *P < 0.05, **P < 0.01, ***P < 0.001. Nonpaired t-test was applied in B, D subpanels 1-3; Mann-Whitney Rank Sum Test was applied in C and D subpanel 4.

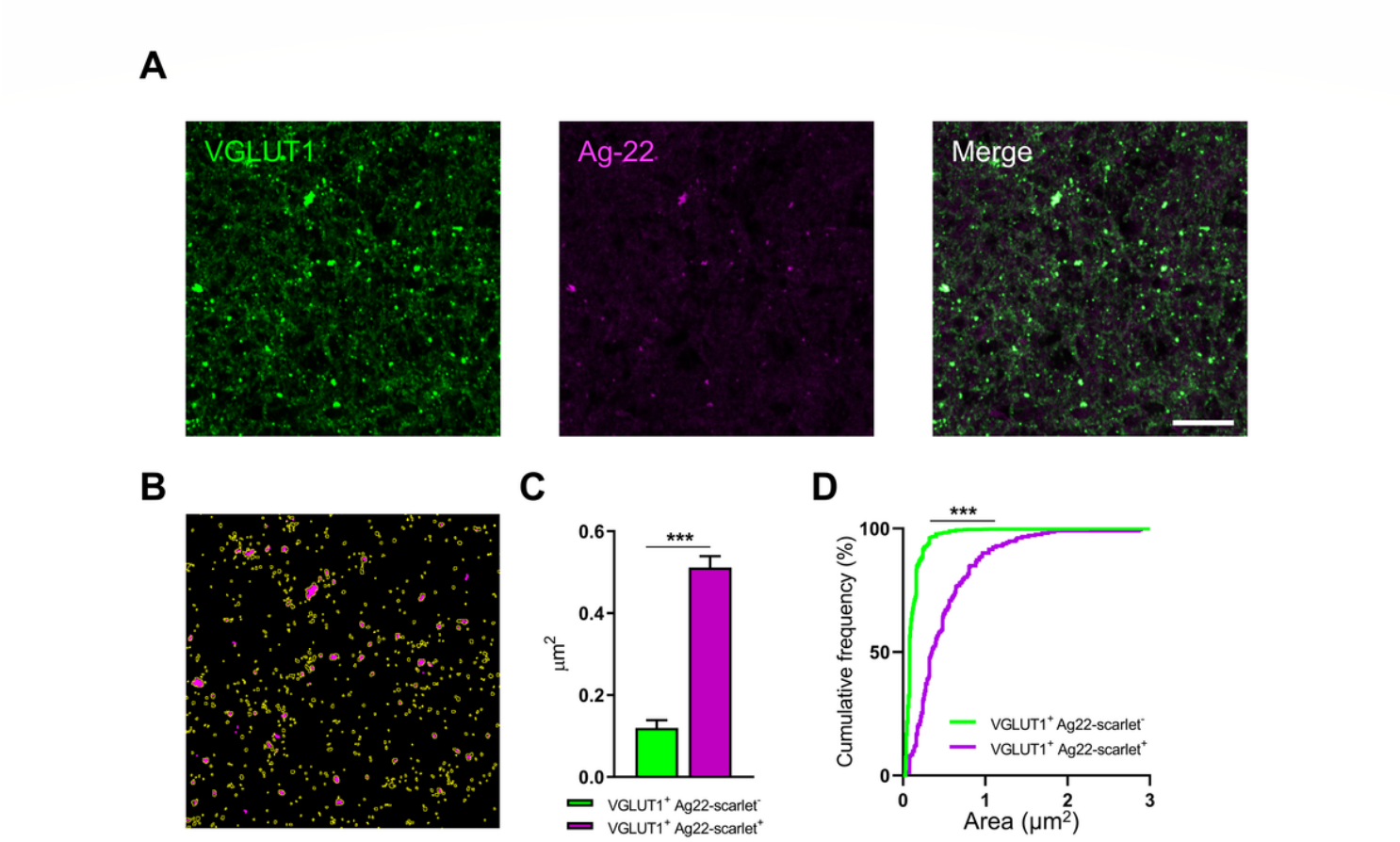

Figure 7

Agrin-22 colocalizes with VGLUT1 in excitatory synapses.

(A) Coimmunostaining of VGLUT1 and agrin-22 (B) ROIs corresponding to the VGLUT1 binary map were superimposed on the Ag22-scarlet binary map to analyze the size of both synaptic populations. (C) Comparison of agrin-22 negative (green) and agrin-22 positive (magenta) areas of VGLUT1$^+$ synapses. (D) Cumulative frequency plot of the Ag22$^+$ and Ag22$^-$ VGLUT1$^+$ presynaptic area. The data are presented as the mean ± SEM values per dendrite. The numbers of analyzed synapses/slices are 1087/3 (VGLUT1$^+$ Ag22-scarlet$^-$) and 214/3 (VGLUT1$^+$ Ag22-scarlet$^+$). ***P < 0.001. Kolmogorov-Smirnov test was applied in D.

Supplementary Files

This is a list of supplementary files associated with this preprint. Click to download.

- FigureS1.tif
- FigureS2.tif
- FigureS3.tif
- FigureS4.tif
- FigureS5.tif
- FigureS6.tif
- FigureS7.tif
- FigureS8.tif
- Supplementaltables.docx